Daniela Helena da Ascenção Loureiro Geraldo Vaqueirinho

Licenciada em Biologia

The role of Arl13b and the non-muscle myosin IIA in cancer cell migration

Dissertação para obtenção do Grau de Mestre em
Genética Molecular e Biomedicina

Orientador: Prof. Dr. Duarte Barral, Investigador Principal no Centro de Estudos de Doenças Crónicas (CEDOC)

FACULDADE DE CIÊNCIAS E TECNOLOGIA
UNIVERSIDADE NOVA DE LISBOA

Setembro 2017

Acknowledgements

Antes de mais, gostaria de agradecer ao Dr. Duarte Barral por me ter aceite como aluna de mestrado no laboratório e, assim, ter tornado possíveis toda a aprendizagem e experiência que adquiri durante este ano. Estou muito grata por poder dizer que tive um excelente orientador, por todo o conhecimento que me transmitiu, todos os conselhos úteis não só para a realização deste trabalho mas também para o meu futuro, toda a disponibilidade e prontidão que sempre demonstrou face a qualquer problema ou questão, todo o acompanhamento que teve o cuidado de realizar continuamente ao longo do ano letivo e ainda pelo esforço que demonstra fazer para manter o grupo unido, dentro e fora do laboratório.

Gostaria de dedicar um agradecimento muito especial à Cristina Casalou, que tive a sorte que me orientasse durante o meu projeto de mestrado. Um enorme obrigada pela excelente orientação que recebi, por todo o conhecimento que me transmitiu desde as bases iniciais aos pequenos detalhes, por todos os conselhos que me ajudaram não só a saber fazer ciência mas também a saber pensar em ciência, por toda a disponibilidade e prontidão que demonstrou para resolver as minhas dúvidas, por toda a paciência com que me ensinou e com que acompanhou também as minhas falhas e ainda por todo o tempo dispensado para esta importante fase da minha formação.

Quero também deixar uma palavra de agradecimento a cada um dos meus colegas de laboratório, que me acompanharam durante este ano. Xana, um grande obrigada por tudo o que me ensinaste, por me ouvires e estares disponível para ajudar e dar sugestões que continuarão a ser úteis daqui para a frente e ainda pela animação e bom humor que trazes ao laboratório. Liliana, um grande obrigada por desde o início me teres feito sentir integrada, pela tua constante prontidão para ajudar, por me ouvires e me aconselhares e pela tua boa disposição. Hugo, muito obrigada por todos os conselhos que sempre estiveste disposto a dar, por teres desde logo contribuído para que sentisse à vontade neste grupo e por tudo aquilo que me ensinaste. Matilde, muito obrigada por toda a prontidão com que te ofereces para colaborar, pelas tuas sugestões sinceras e pelo teu companheirismo. Cristina Escrevente e Cecília, quero deixar-vos também um grande obrigada por estarem sempre disponíveis para me ensinar e ajudar, por todas as sugestões que foram dando ao longo deste ano e que contribuíram para o avanço do meu trabalho e ainda por toda simpatia com que me receberam. Renata e Francisco, apesar de não ter partilhado tanto tempo com vocês, foi também uma honra conhecer-vos e trabalhar com vocês! Finalmente, ao Paul Greiner, com quem foi também uma honra trabalhar e cuja ajuda também quero agradecer.

A todos os membros do laboratório, sem exceção, quero deixar um grande grande obrigada por desde o primeiro dia me terem recebido tão bem e se terem disponibilizado a ensinar-me tudo o que fosse preciso para que me sentisse integrada no laboratório e no CEDOC. Obrigada também por todos os conselhos e por toda a incrível disponibilidade que têm para ajudar. É sem dúvida o vosso

exemplo que quero continuar a seguir em qualquer local onde venha a fazer investigação. Foi uma enorme honra trabalhar em equipa e aprender com todos vocês!

A todos os membros que fizeram parte do laboratório 2.7 durante este ano, obrigada pelo fantástico ambiente de trabalho que se sente e por toda a entreajuda que se verifica. Um obrigada especial às vizinhas do lado, Tatiana, Farzaneh e Catarina por serem tão amorosas e por todos os vossos conselhos e ajuda preciosos!

Obrigada ainda a todas as pessoas do CEDOC por me acolherem e por toda a colaboração que torna o trabalho de todos mais fácil.

Gostaria também de agradecer à coordenadora do Mestrado em Genética Molecular e Biomedicina, a professora Paula Gonçalves, por toda a ajuda, disponibilidade e conselhos.

Finalmente, quero deixar um agradecimento muito muito especial à minha família, amigos e namorado por todo o apoio incondicional e toda a força e alegria que me transmitem, direta ou indiretamente, tornando as minhas aspirações possíveis.

Por todo o conhecimento e experiência com que terminarei o meu Mestrado, por todas as bases que adquiri e com as quais irei continuar a minha carreira científica e pela oportunidade que tive de aprender como fazer um bom trabalho em equipa, não tenho dúvidas de que fiz uma excelente escolha de laboratório e de projeto de investigação para a minha tese de Mestrado. A todos, um grande obrigada por me trazerem até aqui!

Index of contents

Acknowledgements ..... **i**

Index of figures ..... **iii**

Index of tables ..... **v**

Abstract ..... **vii**

Resumo ..... **ix**

Abbreviations ..... **xi**

1. Introduction **1**

1.1. Cell migration 1

1.1.1. Actin-based structures involved in cell migration 2

1.1.2. Retrograde flow and the “molecular clutch” hypothesis 4

1.2. Small GTP-binding proteins and their role in cancer 6

1.2.1. The Arf family 7

1.2.2. The Arl protein Arl13b 8

1.3. NMIIA and cancer cell migration 9

2. Objectives **13**

3. Materials and Methods **15**

3.1. General 15

3.2. Cell culture 15

3.3. Cell migration 15

3.3.1. Stimulation of cell migration stimulation for protein extraction 15

3.3.2. Wound healing assay 15

3.4. Wound healing assay 16

3.5. Cell transfection 16

3.5.1. Overexpression 16

3.5.2. Silencing 17

3.6. RNA extraction, cDNA production and real-time quantitative PCR 17
3.7. Immunofluorescence microscopy 18
3.8. Protein extraction 19
3.9. Immunoprecipitation 19
3.10. SDS-Polyacrylamide Gel Electrophoresis 20
3.11. Immunoblotting 20
3.12. Gel staining 21
3.12.1. Coomassie gel staining 21
3.12.2. Silver nitrate gel staining 21
3.13. Mass spectrometry 22
3.14. Statistical analysis 22
4. Results 23
4.1. Sub-cellular localization of Arl13b and cytoskeleton proteins 23
4.2. Interaction of Arl13b and NMIIA in non-tumorigenic and cancer breast cell lines 26
4.3. Influence of NMIIA silencing on breast cancer cells migratory capacity 31
4.4. Identification of candidate Arl13b interacting partners that can mediate Arl13b function on cell migration 33
5. Discussion 37
References 41
Supplementary information 49

Index of figures

Introduction..... 1

Figure 1.1 – Actin-based structures involved in cell migration. 2

Figure 1.2 – Cellular organization of actin in a migrating cell. 3

Figure 1.3 – The “molecular clutch” hypothesis. 5

Figure 1.4 – The GTP/GDP cycle of small GTP-binding (G) proteins. 7

Figure 1.5 – Structure of the non-muscle myosin II (NMII). 10

Results..... 23

Figure 4.1 – Arl13b co-localizes with actin in MDA-MB-231 cells. 24

Figure 4.2 - Arl13b co-localizes with NMIIA in MDA-MB-231 cells. 25

Figure 4.3 – Arl13b does not co-localize with NMIIB in MDA-MB-231 cells. 26

Figure 4.4 – Co-immunoprecipitation of non-muscular myosin IIA with Arl13b in MDA-MB-231 cells. 26

Figure 4.5 – Co-immunoprecipitation of non-muscular myosin IIA with Arl13b in MDA-MB-231 cells overexpressing Arl13b-GFP. 27

Figure 4.6 – Co-immunoprecipitation of non-muscular myosin IIA with Arl13b in distinct breast cell lines. 28

Figure 4.7 – Co-immunoprecipitation of non-muscular myosin IIA with Arl13b in MCF7 and MCF10A cells during cell migration. 29

Figure 4.8 – Co-immunoprecipitation of non-muscular myosin IIA with Arl13b in GTP bound and unbound conditions. 30

Figure 4.9 – Co-immunoprecipitation of non-muscular myosin IIA with Arl13b in MCF7 cells overexpressing Arl13b-wildtype-GFP or Arl13b-R79Q-GFP. 31

Figure 4.10 – NMIIA silencing leads to increased migration in MDA-MB-231 cells. 32

Figure 4.11 – Silver nitrate staining of gels loaded with Arl13b co-immunoprecipitates. 34

Index of tables

Materials and Methods **15**

Table 3.1 – DNA overexpression plasmids used for MDA-MB-231 transfection 16

Table 3.2 – Sequences of siRNAs used for gene silencing 17

Table 3.3 – Primers used in RT-qPCR 18

Table 3.4 – Primary antibodies used for immunofluorescence 19

Table 3.5 – Secondary antibodies used for immunofluorescence 19

Table 3.6 – Primary antibodies used for immunoblotting 21

Table 3.7 – Secondary antibodies used for immunoblotting 21

Results **23**

Table 4.1 – Mass spectrometry identification of Arl13b-interacting partners that can be involved in Arl13b function in cell migration. 33

Abstract

Cancer metastasis relies on cell migration and invasion of surrounding tissues and is responsible for most cancer-related deaths. Therefore, the study of the molecular mechanisms that govern cell migration and invasion is essential for the development of effective anti-cancer therapies. We previously showed that the small GTP-binding protein Arl13b interacts with the actin cytoskeleton and regulates fibroblast cell migration through the interaction with its effector, the non-muscle myosin heavy chain IIA (NMIIA). Furthermore, we found that Arl13b is required for *in vitro* and *in vivo* migration and invasion of breast cancer cells. The main goal of this work was to assess the NMIIA requirement for the function of Arl13b in cancer cell migration. We found that Arl13b-NMIIA interaction is stronger in migrating cells, and more prominently in the non-tumorigenic breast cell line MCF10A than in the breast cancer cell lines MCF7 and MDA-MB-231. We also found that NMIIA silencing in breast cancer cells does not phenocopy the decrease in cell migration that occurs upon Arl13b silencing. Therefore, we set out to identify new Arl13b-interacting partners that may have a direct association with its role in breast cancer cell migration. Thus, our results provide new insights into the molecular mechanisms of Arl13b in cancer cell migration.

Keywords: Arl13b, non-muscular myosin IIA, cell migration, cancer, actin cytoskeleton.

Resumo

O processo de metastização depende da migração e invasão de células cancerígenas para os tecidos circundantes e é responsável pela maioria das mortes relacionadas com cancro. Por essa razão, o estudo dos mecanismos moleculares de migração e invasão celulares é essencial para o desenvolvimento de terapias mais eficazes para o tratamento de cancro. O nosso grupo descobriu que a proteína G Arl13b interage com o citoesqueleto de actina e regula a migração de fibroblastos através da interação com a proteína efetora miosina não-muscular IIA. Para além disso, descobrimos que a Arl13b é necessária para a migração e invasão de células de cancro de mama *in vitro* e *in vivo*. O principal objetivo deste trabalho foi avaliar a necessidade da NMIIA para a função de Arl13b na migração de células cancerígenas. Descobrimos que a interação entre Arl13b e NMIIA é mais forte em células que estão a migrar, e que isso é mais preponderante na linha celular não-tumorigénica MCF10A do que nas linhas celulares de cancro da mama MCF7 e MDA-MB-231. Descobrímos ainda que o silenciamento da NMIIA nas células de cancro da mama não conduz ao mesmo fenótipo de diminuição da migração celular que se verifica após o silenciamento de Arl13b. Assim, propusemos novas proteínas que interagem com a Arl13b e que possam ter uma relação direta com a sua função na migração de células cancerígenas. Em conclusão, os nossos resultados contribuem para o aprofundamento do conhecimento dos mecanismos moleculares da Arl13b na migração de células cancerígenas.

Palavras-chave: Arl13b, miosina não-muscular IIA, migração celular, cancro, citoesqueleto de actina.

Abbreviations

ANOVA	Analysis of variance
Arf	ADP ribosylation factor
Arl	Arf-like
Arl13b^{hnn}	*Arl13b hennin*
Arp 2/3	Actin-related protein 2/3
ATP	Adenosine triphosphate
BSA	Bovine serum albumin
cDNA	Complementary deoxyribonucleic acid
CDR	Circular Dorsal Ruffle
DAPI	4',6-Diamidino-2-phenylindole
DMEM	Dulbecco's Modified Eagle Medium
dNTP	Deoxyribonucleotide triphosphate
DTT	1,4-Dithiothreitol
E-cadherin	Epithelial cadherin
ECL	Enhanced chemiluminescence
ECM	Extracellular matrix
EDTA	Ethylenediaminetetraacetic acid
EGF	Epidermal growth factor
EGTA	Ethylene glycol-bis(β-aminoethyl ether)-N,N,N',N'-tetraacetic acid
ELC	Essential light chain
Erlin	Endoplasmic reticulum lipid raft-associated protein
FA	Focal adhesion
FBS	Fetal bovine serum
G protein	GTP-binding protein

GAP	GTPase-activating protein
GAPDH	Glyceraldehyde-3-phosphate dehydrogenase
GDI	Guanine nucleotide dissociation inhibitor
GDP	Guanosine diphosphate
GEF	Guanine nucleotide exchange factor
GFP	Green fluorescent protein
GTP	Guanosine triphosphate
HEPES	4-(2-Hydroxyethyl)-1-piperazineethanesulfonic acid
HRP	Horseradish peroxidase
IP	Immunoprecipitation
MLCK	Myosin light chain kinase
mRNA	Messenger ribonucleic acid
MYH	Myosin heavy chain
Nano LC-MS/MS	Nanoscale liquid chromatography coupled to tandem mass spectrometry
NMII	Non-muscle myosin II
N-WASP	Neural-Wiskott-Aldrich syndrome protein
$p(dN)_6$	Deoxyribonucleotide hexamer random primer sequence
PBS	Phosphate buffered saline
PR	Peripheral ruffle
Rab	Ras-like protein in brain
Ran	Ras-like nuclear
Ras	Rat sarcoma
Rho	Ras homologous
RLC	Regulatory light chain
ROCK	RhoA-associated kinase
RT-qPCR	Real-time quantitative polymerase chain reaction

Sar	Secretion associated and Ras-related
SDS	Sodium dodecyl sulfate
SDS-PAGE	SDS-Polyacrylamide Gel Electrophoresis
Ser19	Serine 19
Shh	Sonic hedgehog
siCtrl	siControl
siRNA	Small interfering RNA
Thr18	Threonine 18
Tris	Tris(hydroxymethyl)aminomethane
TX-100	Triton X-100

1. Introduction

1.1. Cell migration

Cell migration is a biological process essential in both physiological and pathological conditions. In early embryonic development, cell migration is required for morphogenetic processes, such as gastrulation (Keller, 2005), and colonization of embryonic tissues by neural crest cells (Locascio and Nieto, 2001). In adulthood, cell migration plays a key role in inflammation (Luster *et al*, 2005) and wound healing (Li, 2013). In fact, the majority of an organism's cell types is able to and undergoes migration at a certain point in space and time (Friedl, 2004).

When cell migration becomes dysregulated, it can lead to pathological conditions, such as cancer metastasis (Wang *et al*, 2005). Metastasis is the result of cancer cell spreading from the tumor's primary site to a distant site in the organism and accounts for the majority of cancer-related cell deaths (Schroeder *et al*, 2011; Fife *et al*, 2014). Therefore, understanding the fundamental mechanisms of cell migration and how tumors subvert this process in order to migrate and invade through tissues is key for understanding cancer progression and developing new therapeutic strategies.

Depending on the cell type and the environmental conditions, there are different mechanisms of cell migration, such as single *versus* collective cell migration or adhesion-dependent *versus* adhesion-independent migration (Friedl, 2004; Friedl *et al*, 2012). In every case, cell migration requires the generation of traction forces by the actin cytoskeleton (Pollard and Cooper, 2009; Case and Waterman, 2015). Thus, actin cytoskeleton remodeling, which comprises the assembly, stabilization and organization of actin filaments, is key for cell migration (Le Clainche and Carlier, 2008).

Cell migration involves a series of coordinated steps that allow cells to adapt and move relatively to their surroundings. Initially, a migrating cell has to undergo polarization (Petrie *et al*, 2009), particularly of the cell cytoskeleton and its associated proteins. This polarization allows dynamic actin structures with protrusive and adhesive functions to form at the cell's leading edge. Hence, migrating cells create extensions, such as lamellipodia and filopodia, which allow protrusion in the direction of migration. Additionally, migrating cells indirectly anchor the actin cytoskeleton to the extracellular matrix (ECM) through the formation of adhesion structures such as focal adhesions (FAs) at the leading edge of the cell, which ultimately allow the traction of the cell body (Gardel *et al*, 2010). Therefore, lamellipodial protrusion and adhesion to the ECM act in an orchestrated manner, usually in response to chemical and physical stimuli (Petrie *et al*, 2009). Lastly, in order to successfully move, the cell has to retract its trailing edge. This is achieved by the simultaneous contractility of the actomyosin network and disassembly of adhesive structures (Le Clainche and Carlier, 2008).

1.1.1. Actin-based structures involved in cell migration

There are several actin-based structures with protrusive and adhesive functions which are considered key players on cell migration (Figure 1.2).

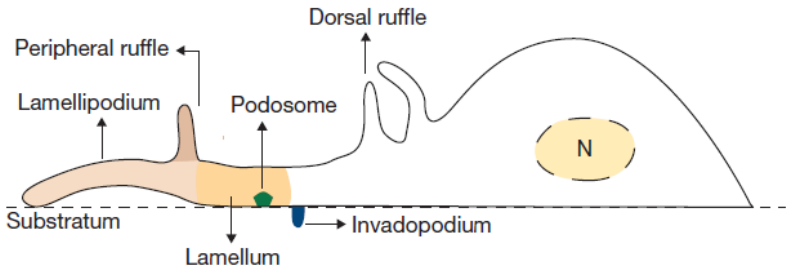

Figure 1.1 – Actin-based structures involved in cell migration. Remodeling of the actin cytoskeleton allows cells to form several structures with different localizations and functions that result in increased migratory capacities. At the leading edge of the migrating cell, protrusive structures such as lamella and lamellipodia are formed by constant actin polymerization. Dorsal ruffles and peripheral ruffles, collectively called membrane ruffles, are non-adhesive structures that can be found at the cell's dorsal surface. Podosomes form at the cell's ventral surface and are characterized by their adhesive and degradative functions. Invadopodia are similar to podosomes, but are characteristic of cancer cells. N, nucleus. Adapted from (Chabra and Higgs, 2007).

The lamellipodium consists of a flat membrane protrusion localized at the migrating cell's leading edge and it is composed of a dense array of branched actin filaments with barbed ends facing the leading edge (Small *et al*, 2002; Case and Waterman, 2015) (Figure 1.2). New actin monomers are constantly incorporated on the barbed end of the actin filament, towards the leading edge. At the same time, there is a constant pointed end depolymerization, which contributes with actin monomers for the elongation. This phenomenon, often referred to as "actin treadmilling", is responsible for the maintenance of the actin filaments of the lamellipodia (Wang *et al*, 1985). The lamella, which is a loose array of unbranched actin filaments located immediately upstream of the lamellipodia (Figure 1.2), has a slower actin turnover (Le Clainche and Carlier, 2008) and is enriched in myosin II and tropomyosin (Gardel *et al*, 2010).

Migrating cells also form filopodia, which are finger-like protrusions that overlap but extend beyond lamellipodia (Le Clainche and Carlier, 2008). These structures are composed of aligned actin filaments and their main function is to sense the extracellular environment and direct the cellular movements (Letort *et al*, 2015) (Figure 1.2). The parallel actin filaments in filopodia also function as tracks for protein intracellular transport (Letort *et al*, 2015). Despite sharing the same cellular environment, filopodia and lamellipodia have different organization and dynamic properties. This can be attributed to the action of different nucleation mechanisms, involving the Actin-related protein (Arp) 2/3 complex or formins, which control the coordinated formation of the two structures (Firat-karalar and Welch, 2012).

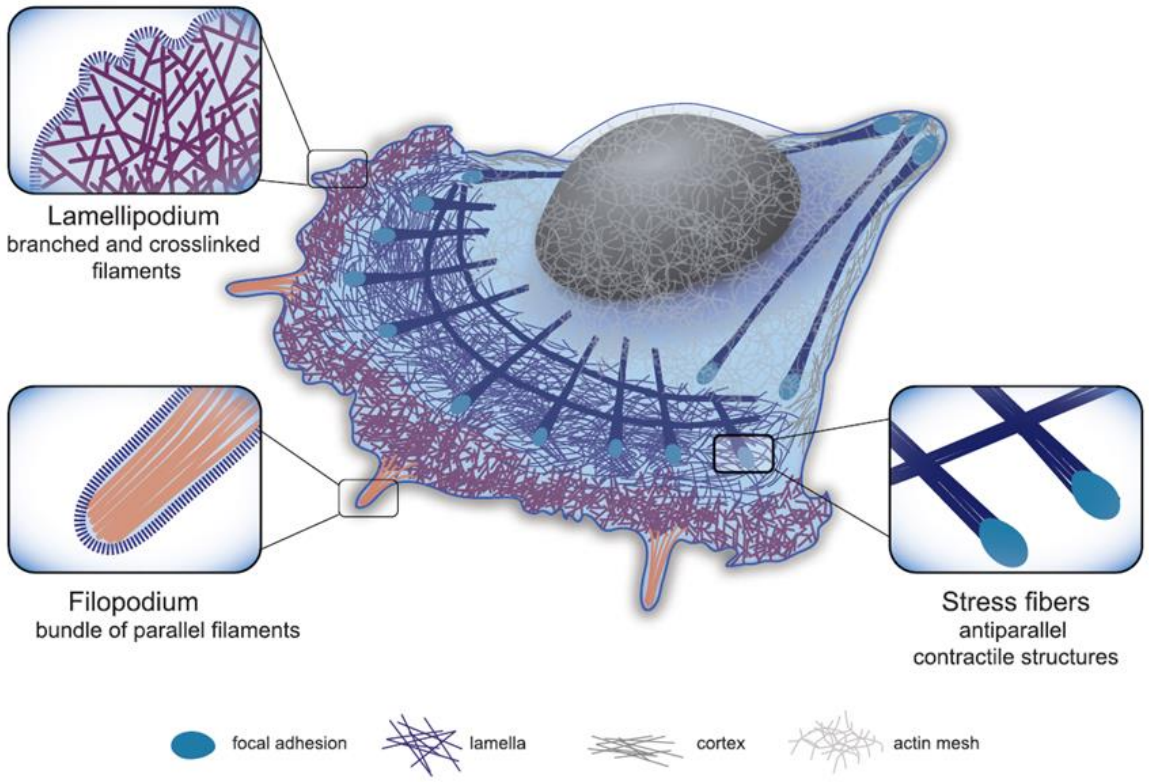

Figure 1.2 – Cellular organization of actin in a migrating cell. The organization and dynamics of the actin cytoskeleton contribute to the formation of protrusive and adhesive structures, which are essential for cell migration. In lamella and lamellipodia, actin is organized in unbranched and branched arrays, respectively. On the other hand, actin filaments in filopodia and stress fibers can be found in bundles of polarized or antiparallel filaments, respectively. Additionally, the filaments in stress fibers are associated with myosin, which gives them contractile properties. Taken from (Letort *et al*, 2015).

The formation of adhesion structures by the migrating cell is also critical for the process of cell migration. Adhesion structures include nascent adhesions, focal complexes, FAs and fibrillar adhesions. Nascent adhesions and focal complexes are the most dynamic, since they have a high assembly/disassembly rate at the edge of the lamellipodium (Wolfenson *et al*, 2013). These are similar structures, essentially distinguished by their myosin dependence and size (Choi *et al*, 2008). Nascent adhesions and focal complexes that do not disassemble undergo maturation, which requires stress fiber assembly and myosin II contractility, and are converted into FAs (Kuo, 2013). These have higher stability and lower adhesion turnover than focal complexes (Le Clainche and Carlier, 2008). Like focal complexes, FAs also localize to the cell periphery. However, FAs have a more central localization and associate with the end of stress fibers, which are contractile bundles of actin, myosin II and bundling proteins such as α-actinin (Le Clainche and Carlier, 2008; Tojkander *et al*, 2012) (Figure 1.2). Finally, fibrillar adhesions are elongated structures associated with fibronectin fibrils that can originate from FAs (Wolfenson *et al*, 2013).

To allow rapid migration, adhesion structures have to be formed at the cell's leading edge and disassembled at the cell's trailing edge (Le Clainche and Carlier, 2008). Integrins, a family of

heterodimeric transmembrane proteins, are an important component of adhesion structures, enabling the connection between the actin cytoskeleton and the ECM (Mayor and Etienne-Manneville, 2016). However, integrins and actin do not bind directly and their association is mediated by the FA, which includes cytoskeletal adaptor proteins such as talin, vinculin and paxillin (Geiger *et al*, 2001; Case and Waterman, 2015).

Besides these specialized structures, many cell types also form other actin-based structures, which are essential for cell migration and invasion, such as podosomes, invadopodia and membrane ruffles (Figure 1.1). Podosomes and invadopodia are structures formed on the cell's ventral surface that are mainly involved in the processes of adhesion and matrix degradation for cell spreading and invasion (Linder, 2007). While podosomes are mostly found in invasive monocytic cells, such as macrophages or dendritic cells, invadopodia are typical of cancer cells (Linder, 2007). Membrane ruffles are non-adhesive structures that extend from the cell's dorsal surface and are subdivided into peripheral ruffles (PRs) and circular dorsal ruffles (CDRs) (Chhabra and Higgs, 2007). PRs extend at the cell's periphery, usually at the leading edge, and move rearward (Abercrombie *et al*, 1970). After assembling at the dorsal surface, CDRs typically expand and then constrict towards their center, maintaining a circular appearance, until they disappear (Krueger *et al*, 2003; Itoh and Hasegawa, 2013). Both types of membrane ruffles have been associated to the process of cell migration (Buccione *et al*, 2004). CDRs, which form transiently upon stimulation by growth factors, are usually implicated in the cell's transition from a static to a migratory phenotype (Mellström *et al*, 1988; Krueger *et al*, 2003; Sero *et al*, 2011). Moreover, they are also associated with membrane receptor internalization and recycling, as well as macropinocytosis (Buccione *et al*, 2004; Hoon *et al*, 2012). In fact, it has been reported that CDRs play a role in FA turnover in migrating cells. Upon FA disassembly, integrins are translocated to CDRs, before being internalized by macropinocytosis and recycled to new focal adhesions at the leading edge of a migrating cell (Gu *et al*, 2011).

1.1.2. Retrograde flow and the "molecular clutch" hypothesis

Cell migration occurs through the coordination of leading edge protrusion, adhesion of the protrusion to the substrate and retraction of the trailing edge. In normal conditions, actin polymerization against the plasma membrane within the lamellipodium results in a counterforce that is thought to push the actin network rearward relatively to the membrane, resulting in a rapid retrograde flow (Ponti, 2004; Case and Waterman, 2015). Additionally, within the lamella, the motor protein myosin II contracts actin bundles, leading to actin reorganization and disassembly, which generate a slower retrograde flow (Ponti, 2004; Case and Waterman, 2015).

In order to convert the polarized actin treadmilling into protrusion force and the actomyosin contraction into traction force, migrating cells form adhesion structures, such as FAs, which act as "molecular clutches" (Burridge and Guilluy, 2016) (Figure 1.3). When the molecular clutch is not engaged, there is no anchorage of the actin cytoskeleton to the substrate. Therefore, the actin

polymerization at the lamellipodium and the actomyosin contraction at the lamella result in net retrograde flow of the actin cytoskeleton and there is no protrusion of the leading edge (Le Clainche and Carlier, 2008). However, when the molecular clutch is engaged, the forces generated by the actin treadmilling and the actomyosin contraction lead instead to a slower retrograde flow, the generation of a traction force on the ECM and net protrusion of the leading edge (Le Clainche and Carlier, 2008). The traction force applied on the cell's stress fibers ultimately leads to the traction of the cell body and retraction of the rear of the cell (Le Clainche and Carlier, 2008).

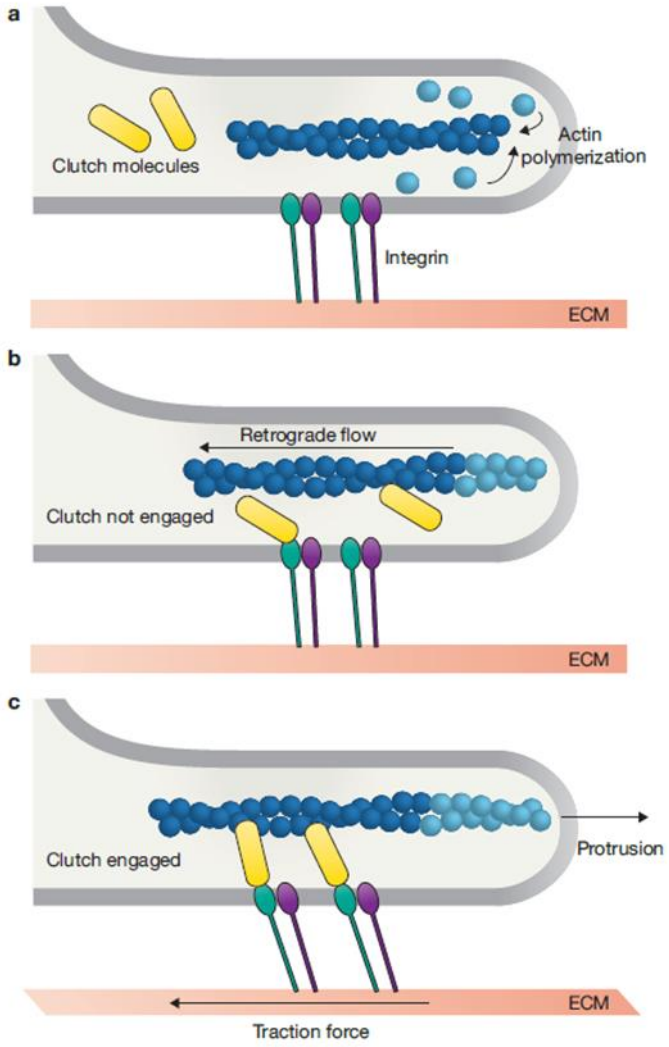

Figure 1.3 – The "molecular clutch" hypothesis. (a) Actin monomers (light blue) are constantly incorporated onto the barbed end of pre-existing actin filaments (dark blue) while depolymerization occurs at the pointed ends in a process called "actin treadmilling". (b) When the actin cytoskeleton is not anchored to the extracellular matrix (ECM) through integrin-based adhesions, the clutch is disengaged and consequently there is no net protrusion. In this case, actin polymerization and actomyosin force are mainly converted into retrograde flow. (c) When the polymerizing actin network is connected to the ECM, the molecular clutch is engaged and actin polymerization and actomyosin contraction are converted into protrusion force and traction force, respectively. Taken from (Case and Waterman, 2015).

Since cell protrusion is dependent on actin treadmilling to push the leading edge membrane, the control of this cycle determines the speed of protrusion. Accordingly, and since the natural treadmilling cycle is too slow to allow rapid migration, there is a set of actin-binding proteins that are able to modulate its speed (Le Clainche and Carlier, 2008). Indeed, there are several proteins that are crucial for the regulation of actin dynamics, including its turnover and remodeling. The Arp2/3 complex and Neural-Wiskott-Aldrich syndrome protein (N-WASP) along with several regulatory elements of the Ras superfamily of small GTP-binding (G) proteins and various actin-capping/binding proteins, such as actin depolymerizing factor, profilin and cofilin, are some of the most important players in the regulation of actin dynamics (Buccione *et al*, 2004).

Alterations in the complex mechanisms that govern the process of cell migration are usually observed in cancer cells with metastatic behavior. In order to successfully mobilize and invade other tissues in the organism, these cells typically undergo modifications in cell shape, cell-cell and cell-ECM adhesion and migratory and invasive capacities (Hanahan and Weinberg, 2011; Fife *et al*, 2014). Moreover, cancer cells stimulate the formation and regulate the turnover of actin-based structures, such as lamellipodia, invadopodia, CDRs and focal adhesions (Yamaguchi and Condeelis, 2007). This is achieved through the manipulation of signaling pathways involved in the actin cytoskeleton reorganization. In fact, several proteins, such as various small G proteins or actin-binding proteins, have already been identified as having altered expression or activity in different cancer types, influencing the metastatic behavior of cancer cells (Yamaguchi and Condeelis, 2007; Fife *et al*, 2014).

1.2. Small GTP-binding proteins and their role in cancer

The Ras (Rat sarcoma) superfamily of GTP-binding (G) proteins is composed of low molecular weight monomeric proteins that bind GTP and are able to hydrolyze it, i.e., they have intrinsic GTPase activity (Goitre *et al*, 2014). In humans, this large superfamily includes over 150 members, which can be further grouped into five major families, based on sequence and functional similarities: Ras, Rho, Rab, Arf and Ran (Goitre *et al*, 2014). All members of this family are binary molecular switches that can be found in two conformational states: a GDP-bound inactive state and a GTP-bound active state (Figure 1.4). Binding to GTP leads to a conformational change that allows small G proteins to bind to their effectors (Herrmann, 2003). In turn, GTP hydrolysis disrupts this interaction, inactivating the small G proteins (Herrmann, 2003).

The GTP hydrolysis activity of the small G proteins is intrinsically low (Goitre *et al*, 2014). However, it can be stimulated by GTPase-activating proteins (GAPs), promoting the inactive conformation (Bernards and Settleman, 2004) (Figure 1.4). Moreover, guanine nucleotide exchange factors (GEFs) promote GDP dissociation, allowing the binding of GTP, which has naturally higher intracellular concentrations than GDP. This promotes the formation of the active GTP-bound state (Schmidt and Hall, 2002). Small G proteins that carry a farnesyl or geranylgeranyl group in their C-terminal domain are additionally regulated by guanine nucleotide dissociation inhibitors (GDIs), which

extract small G proteins from membranes by shielding the hydrophobic tail that is responsible for the membrane association (Cherfils and Zeghouf, 2013). Therefore, this precludes membrane association and interaction with regulators or effectors.

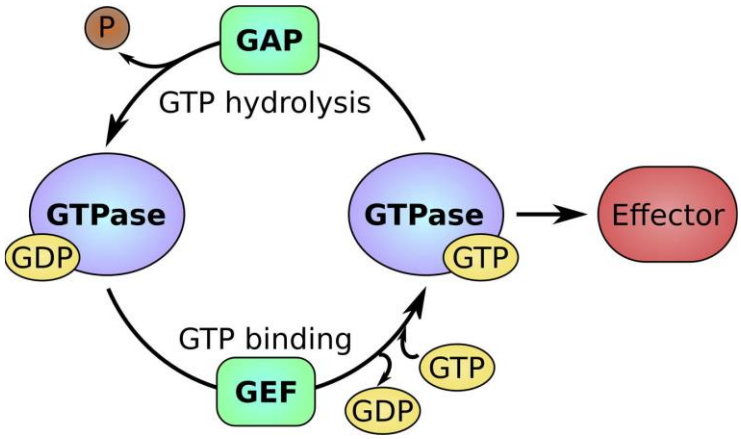

Figure 1.4 – The GTP/GDP cycle of small GTP-binding (G) proteins. Small G proteins can be found in two different states – an active GTP-bound state and an inactive GDP-bound state. The active conformation that results from GTP binding allows small G proteins to interact with their effectors. On the other hand, the inactive conformation does not allow binding to effectors. Small G protein activity is regulated by guanine nucleotide exchange factors (GEFs) and GTPase-activating proteins (GAPs), which can stimulate GDP dissociation and GTPase activity, respectively. P, phosphate. Taken from (Carvalho *et al*, 2015).

Ras superfamily members are associated with several cellular processes, such as proliferation, differentiation, polarity, adhesion and migration. The different families and subfamilies of Ras G proteins regulate distinct biological functions, which is determined by a variation in their sequences and consequently in the effectors and regulators with which they interact (Goitre *et al*, 2014). The different subfamilies also differ in their membrane targeting domains, which determine cellular localization and spatiotemporal regulation (Goitre *et al*, 2014).

Given their crucial role in so many fundamental cellular processes, alterations in the expression and activity of several small G proteins are associated with human diseases (Seixas *et al*, 2013; Casalou *et al*, 2016; Simanshu *et al*, 2017). The Rho (Ras homologous) family members, for example, participate in various signaling networks which influence, among other processes, actin cytoskeleton organization, cell adhesion, polarity and cell migration (Heasman and Ridley, 2008). Thus, deregulation of Rho GTPases is frequently linked to cancer hallmarks, including oncogenic transformation, cell survival and metastasis (Porter *et al*, 2016). Furthermore, the Arf (ADP-ribosylation factor) family of small G proteins has also frequently been described as having a role in cancer progression (Casalou *et al*, 2016).

1.2.1. The Arf family

Besides six mammalian Arf proteins (Arf1-Arf6), the Arf family of small G proteins also comprises the subfamily of Arl (Arf-like), Arp (Arf-related proteins) and the more remotely related Sar

(secretion-associated and Ras-related) proteins (Pasqualato *et al*, 2002). Members of the Arf family are major regulators of intracellular membrane traffic (including vesicle budding, transport and tethering), organelle structure and cytoskeleton organization (Donaldson and Jackson, 2011; Casalou *et al*, 2016). Naturally, since cell migration is highly dependent on polarized vesicle trafficking, protein recycling to the leading edge of migrating cells and actin cytoskeleton dynamics, Arf proteins are also implicated in the regulation of this important cellular process.

Arf and Arl proteins and their modulators of activity (GAPs and GEFs) have emerged as candidate regulators of cancer progression, due to their key roles on various cellular processes that are relevant to the progression of the disease. Namely, they have been shown to modulate cell-cell adhesion (for example, through regulation of E-cadherin internalization and recycling); cellular trafficking of integrins, whose turnover is crucial for cell migration; and actin cytoskeleton remodeling, influencing the formation of actin-dependent structures such as lamellipodia, invadopodia and CDRs (Casalou *et al*, 2016).

1.2.2. Arl13b

Arl13b is an atypical member of the Arl subfamily of Arf small G proteins, which comprises 22 members of generally similar structure (Ivanova *et al*, 2017). While most Arf proteins have a single Arf domain of approximately 20 kDa, Arl13b has an additional 24 kDa C-terminal domain (Larkins *et al*, 2011). Additionally, it does not contain a highly conserved glutamine residue in the nucleotide binding G-3 motif that in other members is necessary for GTPase activity (Ivanova *et al*, 2017). Currently, there are no known Arl13b GAPs or GEFs. Nevertheless, it is known that Arl13b functions as a GEF for Arl3 (Gotthardt *et al*, 2015).

Different missense mutations in *ARL13B* have been identified as causative of the autosomal recessive ciliopathy Joubert syndrome, which is characterized by several developmental defects (Thomas *et al*, 2015). *Arl13b*^{hnn} (*hennin*) mutant mice carry a null mutation of *Arl13b*, which results in defects in cilia structure and Sonic hedgehog (Shh) signaling and is embryonic lethal (Caspary *et al*, 2007). Mouse embryonic fibroblasts derived from these mice have impaired cilia formation, shorter cilia with altered axoneme structure and defects in Shh signaling (Larkins *et al*, 2011).

Besides its known functions in primary cilia development and Shh signaling, our laboratory has demonstrated that Arl13b also regulates endocytic recycling traffic, colocalizes with the actin cytoskeleton and interacts with actin (Barral *et al*, 2012). More recently, it has been shown that this protein is essential for cell migration, as observed *in vitro* in mouse fibroblasts, HeLa and breast and gastric cancer cells and *in vivo* with neural crest cells in zebrafish development and breast cancer mouse models (Casalou *et al*, 2014, 2016; Shao *et al*, 2017; Casalou *et al*, unpublished results). The role of Arl13b in cell migration can be explained at least in part by the fact that it is needed for the formation of CDRs in response to growth factor stimulation, where it associates with the actin cytoskeleton (Casalou

et al, 2014). Finally, Arl13b is also necessary for *in vitro* and *in vivo* breast and gastric cancer cell invasion (Shao *et al*, 2017; Casalou *et al*, unpublished results).

Although the molecular mechanism through which Arl13b regulates cell migration is not yet fully understood, our laboratory has identified the non-muscle myosin heavy chain IIA (NMIIA) as a *bona fide* Arl13b effector in fibroblasts (Casalou *et al*, 2014). Similarly to what was observed for Arl13b, NMIIA has also demonstrated to be necessary for CDR formation, where it colocalizes with Arl13b and actin (Casalou *et al*, 2014). Furthermore, NMIIA is essential for the interaction between Arl13b and actin (Casalou *et al*, 2014).

1.3. NMIIA and cancer cell migration

Non-muscle myosin II (NMII) is part of the myosin superfamily, which comprises a group of motor proteins with key roles in cellular processes that depend on force and translocation (Vicente-Manzanares *et al*, 2009). Many NMII functions are possible due to its interaction with actin and its ability to walk along actin filaments, crosslink them and slide them past each other (Vicente-Manzanares *et al*, 2009; Newell-Litwa *et al*, 2015). This sliding, in turn, allows contraction and generation of tension force on actomyosin filament bundles (Vicente-Manzanares *et al*, 2009; Newell-Litwa *et al*, 2015).

Each NMII molecule is composed of two heavy chains, two regulatory light chains (RLC) and two essential light chains (ELC) (Chen *et al*, 2016) (Figure 1.5). The heavy chain includes a globular head domain, which binds actin and has ATPase activity; a neck domain, which binds RLC and ELC; and a tail domain, with a region of helical homodimerization and a short non-helical tail (Winkelmann *et al*, 1984; Rayment *et al*, 1993a, 1993b; Sandquist and Means, 2008). There are three NMII heavy chain isoforms (A, B and C), which in mammalian cells are encoded by the *MYH9*, *MYH10* and *MYH14* genes, respectively (Newell-Litwa *et al*, 2015). The NMII isoform – NMIIA, NMIIB and NMIIC – is determined by the isoform of the heavy chain that it contains, and since they form homodimers, deletion of a specific heavy chain isoform leads to loss of the respective NMII isoform (Vicente-Manzanares *et al*, 2009).

The RLC allows regulation of NMII conformation and activity, which depends on its state of phosphorylation on Ser19 and/or Thr18 (Umemoto *et al*, 1989). Phosphorylation of both residues leads to a conformational change that causes increased association with actin, ATPase activity and actomyosin filament formation (Scholey *et al*, 1980; Umemoto *et al*, 1989; Vicente-Manzanares and Horwitz, 2010). Finally, the function of ELC is to stabilize the heavy chain (Vicente-Manzanares *et al*, 2009).

There are several known regulators of NMII activity, namely various kinases, such as RhoA-associated kinase (ROCK) and myosin light chain kinase (MLCK), which function downstream of different signaling pathways, such as those associated with small Rho G proteins and Ca^{2+} (Somlyo and Somlyo, 2003; Heasman and Ridley, 2008).

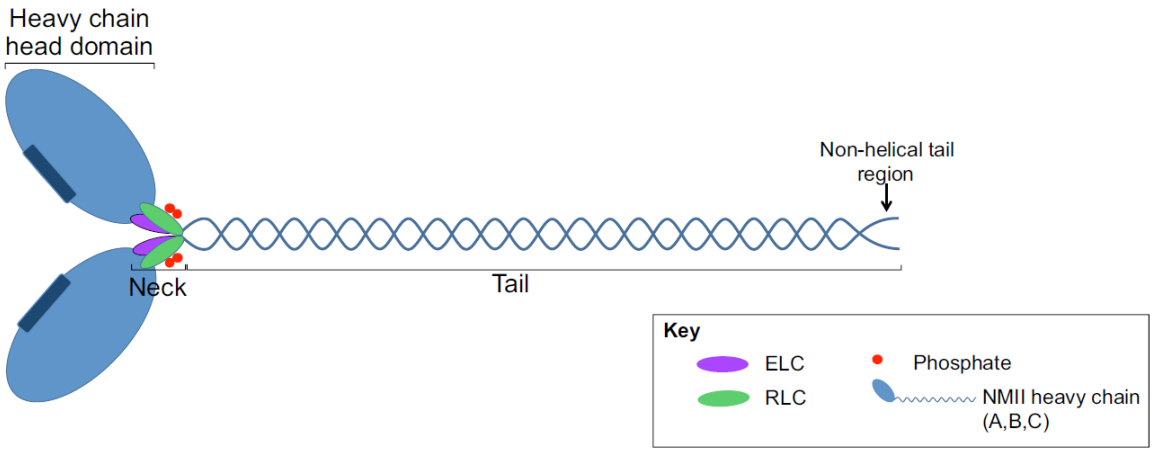

Figure 1.5 – Structure of the non-muscle myosin II (NMII). NMII comprises two heavy chains, two essential light chains (ELC) and two regulatory light chains (RLC). The heavy chain molecules contain a globular head domain, with actin-binding regions and ATPase activity; a neck domain, to which ELC and RLC bind; and a tail domain, which has a helical region, where dimerization occurs, and a non-helical region. RLC can be phosphorylated on the Ser19 and Thr18 domains, which regulates NMII activity. Adapted from (Newell-Litwa *et al*, 2015).

NMII is necessary for many essential cellular processes, such as cell division, polarity, migration and adhesion. Therefore, altered NMII expression and activity contributes to several pathologies, including neuronal disorders, cancer and cardiovascular diseases (Ma and Adelstein, 2014). In fact, differential expression and/or activation of NMII isoforms have been observed in several types of cancer, either due to alterations on the genes that encode NMII or its regulatory proteins. The development of cancer phenotypes has been attributed to NMII-associated changes in cell division, differentiation, apoptosis, cell-cell and cell-matrix adhesion and motility (Newell-Litwa *et al*, 2015). However, NMII does not always have the same role in distinct types of cancer. Although poor prognosis is frequently associated with upregulation or increased activation of NMII, various cancer types and conditions present decreased expression and/or activity of NMII and associated regulators (Newell-Litwa *et al*, 2015).

Many studies have investigated the role of NMII in cell migration. In fact, there are several mechanisms through which NMII regulates this process. During cell migration, distinct NMII isoforms show different subcellular distributions and localized activities. For example, NMIIA generally localizes to the cell's leading edge, where it regulates actomyosin contraction and adhesion maturation, whereas NMIIB usually mediates contraction at the cell's trailing edge and has also a role on adhesion maturation, nucleus orientation and detachment from the ECM (Vicente-Manzanares *et al*, 2007). NMIIA has also been reported to mediate retraction of the trailing edge (Vicente-Manzanares *et al*, 2009). Furthermore, during collective cell migration, NMII is highly expressed in border cells and contributes to the generation of traction forces that drag the following cells (Gaggioli *et al*, 2007; Combedazou *et al*, 2016).

NMIIA does not have a relevant localization or function at the lamellipodium, but instead localizes and influences the actin retrograde flow at the lamella, as mentioned above. It has been

observed in several cell types that NMII induces periodic contractions of the lamellipodium during the advancement of the leading edge, which could contribute to a decrease in the protrusion rate (Vicente-Manzanares *et al*, 2007, 2009). Upon inhibition of NMII with blebbistatin or deletion of the corresponding gene, the periodic contractions are absent, the retrograde flow at the lamella decreases and protrusiveness increases (Vicente-Manzanares *et al*, 2009).

NMII is also important in the control of integrin-mediated adhesion, which is also essential for cell migration. Although NMII is dispensable for the turnover of nascent adhesions at the lamellipodium, it is required for their maturation, through actin bundling and contractile activity (Choi *et al*, 2008). In fact, higher levels of active NMII lead to an increased likelihood that a nascent adhesion undergoes maturation instead of disassembly (Choi *et al*, 2008). Moreover, NMII depletion leads to decreased numbers of large FAs, while it has less effect on small adhesions (Jorrisch *et al*, 2013; Chen *et al*, 2016).

Distinct cell types show different roles for NMII on cell migration. For example, highly migratory cells, such as leukocytes, do not usually form large adhesion structures, which can be associated to low levels of NMII activation (Vicente-Manzanares *et al*, 2009). On the other hand, adhesions of mildly migratory cells, such as fibroblasts, tend to undergo maturation to large and elongated structures, which can be associated to NMII activation (Vicente-Manzanares *et al*, 2009). In fact, *in vitro* two-dimensional migration assays with NMIIA-depleted cells have frequently led to contradictory results. While in some cell types, NMIIA deficiency leads to impaired cell migration (Betapudi *et al*, 2006; Casalou *et al*, 2014; Liu *et al*, 2015), in others it results in increased migratory capacity (Sandquist *et al*, 2006; Even-Ram *et al*, 2007; Doyle *et al*, 2012; Jorrisch *et al*, 2013). Even in the same cell type, such as NIH/3T3 fibroblasts, opposing phenotypes have been observed, which can be explained by differences in the employed assays, distinct experimental conditions and/or genotypic or phenotypic drifts of the cell lines (Casalou *et al*., 2014; Chen *et al*., 2016).

It has been observed that NMIIA-deficient cells adhere to the substrate without distinct focal adhesions or actin stress fibers and migrate faster and more persistently than wildtype or NMIIB-deficient cells (Jorrisch *et al*, 2013). Additionally, NMIIA-deficient cells exert significantly reduced traction forces on the substrates, while NMIIB-deficient cells exert traction forces similar to wildtype cells (Jorrisch *et al*, 2013). This could be due to the increase in intracellular actin monomer availability deriving from the absence of actin stress fibers and promoting actin polymerization, or to the decreased requirement for contractile retraction force deriving from the absence of strong adhesion structures (Jorrisch *et al*, 2013).

Thus, given all the variations observed in the roles of NMII in different contexts, such as type of cancer, cell type and mode of migration, it is important to understand the specific molecular mechanisms that are employed by a given cancer or cell type. This will provide information about how fundamental/prevailing the mechanism is and, consequently, how suitable it is for therapeutic approaches.

2. Objectives

As described above, previous results from our laboratory have uncovered a role for Arl13b in breast cancer cell migration and invasion. Indeed, Arl13b silencing decreases the migration and invasion of highly invasive MDA-MB-231 and poorly invasive MCF7 breast cancer cells (Casalou *et al*, unpublished results). Accordingly, Arl13b overexpression leads to the opposite phenotype. Furthermore, it has previously been shown that Arl13b is involved in the regulation of the actin cytoskeleton dynamics in cell migration, through the interaction with its effector, the non-muscle myosin IIA (Casalou *et al*, 2014). Considering these results, the main goal of this work was **to assess the NMIIA requirement for the function of Arl13b in breast cancer cell migration**, thus contributing to the unraveling of the molecular mechanisms of Arl13b in cancer cell migration.

Specific aim 1: **Assess Arl13b colocalization with actin and NMII isoforms and interaction with NMIIA in breast cell lines**

As described above, although cell migration depends on the formation and action of conserved structures and proteins, some variations can be observed on the molecular mechanisms of cell migration in different cell types. Therefore, we aimed to visualize the colocalization of Arl13b, actin and NMII isoforms in breast cancer cells, which had already been observed in fibroblasts (Casalou *et al*, 2014), and study the importance of Arl13b-NMIIA interaction in the motility of breast cells with different migratory capacities.

Specific aim 2: **Determine if Arl13b regulates the migratory capacity of breast cancer cells through its effector NMIIA**

Since the silencing of Arl13b leads to a decrease in the migratory capacity of breast cancer cells, we aimed to assess if the same phenotype is obtained upon NMIIA silencing.

Specific aim 2: **Identify new Arl13b-interacting partners with a direct role in breast cancer cell migration**

Since the ultimate goal of this project was to characterize the molecular mechanisms of Arl13b in cancer progression, we also aimed to find new candidate proteins that can mediate the function of Arl13b in breast cancer cell migration.

3. Materials and Methods

3.1. General

All reagents were purchased from Sigma-Aldrich unless otherwise stated.

3.2. Cell culture

MDA-MB-231 and MCF7 breast cancer cells were incubated at 37ºC and 5% CO_2 and cultured in Dulbecco's Modified Eagle's Medium (DMEM; Gibco) supplemented with 10% heat-inactivated fetal bovine serum (FBS; Gibco), 100 U/mL penicillin-streptomycin (Gibco), 2 mM GlutaMAX (Gibco) and 15 mM HEPES (Gibco) (DMEM Complete medium).

MCF10A breast cells were incubated at 37ºC and 5% CO_2 and cultured with DMEM/F-12 medium (Gibco) supplemented with 7.5% heat-inactivated horse serum, 100 U/mL penicillin-streptomycin (Gibco), 10 µg/mL insulin, 0.1 µg/mL cholera toxin, 0.5 µg/mL hydrocortisone and 20 µg/mL EGF.

3.3. Cell migration

3.3.1. Stimulation of cell migration stimulation for protein extraction

To stimulate cell migration for protein extraction from migrating cells, MDA-MB-231, MCF7 or MCF10A cells were grown to a confluent monolayer in DMEM Complete medium before replacing the medium by DMEM supplemented with 0,5% BSA, 2 mM GlutaMAX and 15 mM HEPES (serum-free DMEM) and incubating the cells for 18 hours at 37ºC and 5% CO_2. Multiple wound scratches were made on the confluent monolayers with 200 µL tips and a multichannel pipette and serum-free DMEM was replaced by DMEM Complete medium. After 1 to 2 hours of migration at 37ºC and 5% CO_2, cells were collected for protein extraction.

3.3.2. Wound healing assay

After siRNA transfection, MDA-MB-231 or MCF7 cells were grown to a confluent monolayer in a 24-well plate in DMEM Complete medium. When cells were nearly confluent, growth media was replaced by serum-free DMEM and cells were incubated overnight at 37ºC and 5% CO_2. After a single scratch using a 200 µL pipette tip, cells were washed once with PBS and growth media was replaced by DMEM Complete medium. Images were taken from each well immediately (t (time) = 0h) and 4 (t = 4h) and 8 (t = 8h) hours after the scratching using an Axiovert 40 CFL inverted microscope. The area of

the wounds at the different time points was measured using the ImageJ software. Percentage of wound closure was determined as follows: [1 – (wound area at t = 4h or t = 8h / wound area at t = 0h) x 100].

3.4. Wound healing assay

After siRNA transfection, MDA-MB-231 or MCF7 cells were grown to a confluent monolayer in a 24-well plate in DMEM Complete medium. When cells were nearly confluent, the medium was replaced by serum-free DMEM and cells were incubated overnight at 37ºC and 5% CO_2. After a single scratch using a 200 µL pipette tip, cells were washed once with PBS and growth media was replaced by DMEM Complete medium. Images were taken from each well immediately (t = 0h) and 4 (t = 4h) and 8 (t = 8h) hours after the scratching using an Axiovert 40 CFL inverted microscope. The area of the wounds at the different time points was measured using ImageJ software. The percentage of wound closure was determined as follows: [1 – (wound area at t = 4h or t = 8h / wound area at t = 0h) x 100].

3.5. Cell transfection

3.5.1. Overexpression

MDA-MB-231 cells (1.25 x 10^5 cells/well) were seeded 24 hours before transfection in 24-well plates with a glass coverslip (ø 13 mm) and cultured in DMEM Complete medium. Before transfection, the medium was exchanged for Opti-MEM (Gibco). The cells were then transfected with 1.5 µg DNA and 1.5 µL Lipofectamine 2000 (Invitrogen) in 100 µL (final volume) Opti-MEM, according to the manufacturer's instructions. The DNA plasmids used are listed in Table 3.1. Four hours after transfection, the medium was replaced by DMEM Complete medium and cells were incubated at 37ºC and 5% CO_2 for 24 hours.

All overexpression plasmids were produced and purified from transformed *Escherichia coli* glycerol stocks, using the Plasmid Midi Kit for DNA purification (QIAGEN) according to the manufacturer's instructions.

Table 3.1 – DNA overexpression plasmids used for MDA-MB-231 transfection

Gene	**Plasmid**
GFP	pEGFP-C3
ARL13b (wildtype)	pEGFP-C-CMV5-Arl13b
ARL13b-R79Q	pEGFP-C-CMV5-Arl13b-R79Q
MYH9	CMV-GFP-NMHC-IIA
MYH10	CMV-GFP-NMHC-IIB

3.5.2. Silencing

NMIIA and NMIIB were silenced using siGENOME SMARTpool oligonucleotides (Dharmacon) specific for the human genes (*MYH9* and *MYH10*, respectively). The sequences of small interfering RNAs (siRNAs) used are listed in Table 3.2. MDA-MB-231 cells (8 x 10^4 cells/well) were seeded 24 hours before transfection in 24-well plates and cultured in DMEM Complete medium. Transfection was performed using 20 μM siRNA and 1 μL DharmaFECT 4 (Dharmacon) in 100 μL (final volume) Opti-MEM, according to the manufacturer's instructions. Sixteen hours after transfection, the medium was replaced by DMEM Complete medium and cells were incubated at 37ºC and 5% CO_2.

Table 3.2 – Sequences of siRNAs used for gene silencing

siRNA	siRNA sequence
siControl	UAAGGCUAUGAAGAGAUAC
siMYH9	UCAGAAACCUCGACAAUUA;
	GAAUGAAGCUUCCGUUUUA;
	GAUCCGGGCUUUAGAAUUG;
	GAGAACACCUAAAGUCUGA
siMYH10	GAAGUCAGCUCCCUAAAGA;
	GCACAGAGCUGGCCGACAA;
	GGCCAAACCUGCCGAAUAA;
	GAACAUGGCCCUCAAGAAG

3.6. RNA extraction, cDNA production and real-time quantitative PCR

RNA from MDA-MB-231 or MCF7 cells was extracted using the RNeasy Mini Kit (QIAGEN) according to the manufacturer's instructions. Total RNA (500 ng) was transcribed into complementary DNA (cDNA) by incubation with 0.8 mM of dNTP mix (Thermo Scientific) and 0.25 μg/μL of random primers $p(dN)_6$ (Roche) at 65ºC for 5 minutes. After placing the samples on ice for a few seconds, they were incubated with 1x first-strand buffer (Invitrogen), 10 mM of DTT (Invitrogen) and 2 U/μL of RNaseOUT Recombinant Ribonuclease Inhibitor (Invitrogen) at 25ºC for 2 minutes. Finally, 2.5 U/μL of SuperScript II Reverse Transcriptase (Invitrogen) were added and samples were incubated at 25ºC for 10 minutes, at 42ºC for 50 minutes and at 70ºC for 15 minutes.

Real-time quantitative PCR (RT-qPCR) was performed in a qPCR LightCycler (Roche), using the FastStart Essential DNA Green Master kit (Roche) according to the manufacturer's instructions. Amplification of the *GAPDH* housekeeping gene was done as an endogenous control for normalization of the expression level of each analyzed gene. The used primers are all specific for the human genes and are listed in Table 3.3. Analysis of the RT-qPCR data was done using the Roche LightCycler 96 software.

Table 3.3 – Primers used in RT-qPCR

Gene	**Primer sequence (5'-3')**
GAPDH	Forward: CATTTCCTGGTATGACAACGA
	Reverse: GTCTACATGGCAACTGTGAG
MYH9	Forward: AGAAGGTGAAGGTGAACAAGG
	Reverse: GGTGTAGATGAGCCCTGAGTAG
MYH10	Forward: AGCCCAGACCAAAGAACAG
	Reverse: ATGAAAGATGTCCCTGACG

3.7. Immunofluorescence microscopy

MDA-MB-231 cells (1.25 x 10^5 cells/well) were seeded on glass coverslips (ø 13 mm) in a 24-well plate and transfected as described previously. Twenty-four hours after transfection, the medium was removed and cells were fixed with 4% paraformaldehyde (Alfa Aesar) in PBS during 15 minutes at room temperature. After washing 3 times with PBS, the cells were blocked and permeabilized with 1% BSA and 0.05% saponin in PBS (blocking/permeabilization solution) for 30 minutes at room temperature. Cells were then incubated with the primary antibodies diluted in blocking/permeabilization solution for 60 minutes at room temperature in a humidified chamber. Coverslips were washed 5 times with PBS and incubated with the secondary antibodies or Alexa-Fluor-568-conjugated phalloidin diluted in the blocking/permeabilization solution for 60 minutes at room temperature in a humidified chamber. After 4 washes with PBS, cells were incubated with 1 µg/mL DAPI diluted in PBS for 5 minutes. Finally, coverslips were mounted in mounting media containing 10% Mowiol 4-88 in 100 mM Tris-HCl (pH = 8.5) and 25% glycerol. Images were acquired with a ZEISS LSM 710 confocal laser scanning microscope with a Plan-Apochromat 63x/1.4 NA oil-immersion objective and processed with the ImageJ software. The primary and secondary antibodies used are listed in Table 3.4 and Table 3.5, respectively.

Table 3.4 – Primary antibodies used for immunofluorescence

Antibody	Host species	Recognized antigen	Source	Final concentration/Dilution
anti-NMIIA	Rabbit	NMIIA	Sigma	6.75 µg/mL
anti-NMIIB	Mouse	NMIIB	Abcam	1:100

Table 3.5 – Secondary antibodies used for immunofluorescence

Antibody	Host species	Label	Source	Final concentration
anti-mouse	Goat	Alexa Fluor 568	Invitrogen	2 µg/mL
anti-rabbit	Goat	Alexa Fluor 568	Invitrogen	2 µg/mL

3.8. Protein extraction

MDA-MB-231, MCF7 or MCF10A cells were lysed with ice-cold lysis buffer containing 50 mM Tris-HCl (pH = 7.5), 1 mM EDTA, 1 mM EGTA, 150 mM NaCl, 2 mM $MgCl_2$, 1 mM DTT and either 1% IGEPAL or 0.1% TX-100. Immediately before use, the buffer was supplemented with 1x cOmplete (Roche) protease inhibitor cocktail and 1 µM sodium orthovanadate and cells were incubated with the supplemented lysis buffer for 30 minutes on ice. After centrifugation at 13,800 x *g* for 30 minutes at 4ºC, the supernatants were collected. Protein concentration was determined using the DC Protein Assay kit (Bio-Rad), according to the manufacturer's instructions.

3.9. Immunoprecipitation

For Arl13b immunoprecipitation, 800 to 1,500 µg of total protein extract were pre-cleared with Protein G-Sepharose 4 Fast Flow beads (GE Healthcare) for 1 hour at 4ºC, with rotation. Immunoprecipitation was performed overnight at 4ºC with rotation, using 3 µg of rabbit anti-Arl13b antibody (Barral *et al*, 2012). Protein G-Sepharose 4 Fast Flow beads were then added and incubated for 4 to 5 hours at 4ºC with rotation. The samples were centrifuged at 13,800 x *g* for 5 minutes at 4ºC and the supernatant was discarded. The pellet was washed once with lysis buffer containing 500 mM NaCl and three times with lysis buffer containing 150 mM NaCl. Finally, samples were solubilized in 2x sample buffer (20 mM sodium phosphate, 2% SDS, 0.001 % bromophenol blue, 0.2 M DTT and 2% glycerol) supplemented with 1,43 M β-mercaptoethanol, boiled at 95ºC for 5 minutes and centrifuged at 13,800 x *g* for 5 minutes at 4ºC. The supernatant containing immunoprecipitated proteins was collected and analyzed.

For the immunoprecipitation involving GTPɣS or GDP loading, 0.5 mM GTPɣS or 5 mM GDP were added to the pre-cleared protein extracts for 15 minutes at room temperature with agitation, before incubation with the antibody.

For GFP-tagged Arl13b immunoprecipitation performed by Paul Greiner and Cristina Casalou, GFP-Trap beads (ChromoTek) were equilibrated in lysis buffer containing 150 mM NaCl, before incubation with 500 µg of total protein extract for 2 hours at 4ºC. The samples were then centrifuged at 2,500 x *g* for 3 minutes at 4ºC, and the supernatants were discarded. The beads were then washed once with lysis buffer containing 500 mM NaCl and three times with lysis buffer containing 150 mM NaCl. Finally, samples were solubilized in 2x sample buffer supplemented with 1,43 M β-mercaptoethanol, boiled at 95ºC for 5 minutes and centrifuged at 13,800 x *g* for 5 minutes at 4ºC. The supernatant containing immunoprecipitated proteins was collected and analyzed.

3.10. SDS-Polyacrylamide Gel Electrophoresis

Tris-glycine sodium dodecyl sulfate (SDS)-polyacrylamide gels containing 8% polyacrylamide resolving gel (pH= 8.8) and 5% polyacrylamide stacking gel (pH = 6.8) were prepared using a 1 mm spacer, mounted in the gel electrophoresis system (Amersham Biosciences) and covered with running buffer containing 25 mM Trizma base, 192 mM glycine and 0,1% SDS. Protein samples previously solubilized in 2x sample buffer supplemented with 1,43 M β-mercaptoethanol and boiled at 95ºC for 5 minutes were applied on the gel along with 10 µL Precision Plus All Blue Protein Standards (Bio-Rad). SDS-Polyacrylamide Gel Electrophoresis was performed at 20 mA per running gel during 1 to 2 hours.

3.11. Immunoblotting

Protein samples separated on an 8% SDS-PAGE gel were transferred onto a nitrocellulose blotting membrane (0.45 µm pore; GE Healthcare) in transfer buffer containing 25 mM Trizma base, 192 mM glycine, 0.25% SDS and 20% ethanol for 75 minutes at 100V. Membranes were blocked in blocking buffer (5% non-fat dried milk and 0.1% Tween-20 in PBS) for 1 hour at room temperature, before incubation with primary antibodies in a humidified chamber for 1 hour at room temperature. Membranes were then washed 3 times for 5 minutes in 0.1% Tween-20 in PBS and incubated with HRP-conjugated secondary antibodies for 1 hour at room temperature under constant agitation. Finally, membranes were washed 3 times for 5 min in 0.1% Tween-20 in PBS and the antibodies were detected using Amersham ECL Select (GE Healthcare), according to the manufacturer's instructions. Chemiluminescence was detected using the ChemiDoc Touch Imaging System. Band intensities were quantified using the ImageJ software and normalized using GAPDH as a loading control. The primary and secondary antibodies were diluted in blocking buffer and are listed in Table 3.6 and Table 3.7, respectively.

Table 3.6 – Primary antibodies used for immunoblotting

Antibody	Host species	Recognized antigen	Source	Final concentration
anti-Arl13b	Rabbit	Arl13b	(Barral *et al*, 2012)	4 µg/mL
anti-GAPDH	Goat	GAPDH	SICGEN	2 µg/mL
anti-GFP	Goat	GFP	SICGEN	2 µg/mL
anti-NMIIA	Rabbit	NMIIA	Sigma	0.675 µg/mL

Table 3.7 – Secondary antibodies used for immunoblotting

Antibody	Host species	Label	Source	Final concentration/Dilution
Anti-rabbit	Donkey	HRP	GE Healthcare	1:5,000
Anti-rabbit - light chain specific	Mouse	HRP	Jackson ImmunoResearch	0.16 µg/mL
Anti-goat	Donkey	HRP	Jackson ImmunoResearch	0.16 µg/mL

3.12. Gel staining

3.12.1. Coomassie gel staining

Immunoprecipitated proteins were analyzed on an 8% SDS-PAGE gel. The gel was fixed with a 40% ethanol and 10% acetic acid solution for 1 hour with agitation, before washing twice with distilled water for 10 minutes with agitation. The gel was stained in 0.12% Coomassie Brilliant Blue G-250 or Coomassie Brilliant Blue R-250, 10% orthophosphoric acid, 10% ammonium sulfate and 20% anhydrous methanol, overnight at room temperature with constant agitation. Finally, the gel was washed with a 1% acetic acid solution with agitation until the background was clear.

3.12.2. Silver nitrate gel staining

Following Coomassie staining, the gel was incubated with a 50% methanol and 5% acetic acid solution for 30 minutes with agitation, before washing twice for 2 minutes and once for 2 hours with agitation in distilled water. The gel was incubated with 0.02% sodium thiosulfate (pentahydrate) for

2 minutes before incubation with cold 0.1% silver nitrate for 30 minutes with agitation. After washing twice for 30 seconds with distilled water, the gel was incubated with 2% anhydrous sodium carbonate and 0.04% formaldehyde. When all bands were clearly visible, the reaction was stopped using a 1% acetic acid solution.

3.13. Mass spectrometry

Mass spectrometry analysis was performed at the ITQB (Instituto de Tecnologia Química e Biológica António Xavier) Mass Spectrometry Unit (UniMS). Individual immunoprecipitated bands of interest excised from the silver nitrate stained gel were digested with trypsin before protein desalting and concentration in C18 micro-columns. Nanoscale liquid chromatography coupled to tandem mass spectrometry (nano LC-MS/MS) runs of 45 minutes were performed using a TripleTOF 6600 mass spectrometry system (SCIEX). Protein identification was obtained by screening in protein sequence databases.

3.14. Statistical analysis

Numerical data are presented as mean ± standard deviation for wound healing assays and RT-qPCR. One-way ANOVA with Dunnett's multiple comparison test was used to analyze the distinct wound healing assays data sets relatively to siControl. Statistical analysis was performed using GraphPad Prism software (version 7.03).

4. Results

4.1. Sub-cellular localization of Arl13b and cytoskeleton proteins

Interaction and co-localization of the actin cytoskeleton and the NMII isoforms NMIIA and NMIIB is conserved between different types of cells. Previous results from our laboratory have shown that the small G protein Arl13b co-localizes with actin and NMIIA in mouse fibroblasts (Casalou *et al*, 2014). In these cells, Arl13b interacts with actin and NMIIA, which proved to be required for cell migration. Since cells with different migratory capacities often show variation on the molecular mechanisms used for cell migration, co-localization of Arl13b with actin, NMIIA or NMIIB was assessed on the highly migratory MDA-MB-231 cells by confocal microscopy. Immunocytochemistry was performed using phalloidin to visualize filamentous actin and NMIIA or NMIIB antibodies to visualize the respective proteins. MDA-MB-231 cells overexpressing GFP-tagged Arl13b, NMIIA or NMIIB were also used to assess the localization of these proteins.

We observed that Arl13b co-localizes with actin, especially with structures localized near the cell periphery and at the plasma membrane (Figure 4.1A and B). It is also interesting to note the presence of Arl13b-positive vesicles surrounded by actin (Figure 4.1C and D). Arl13b also co-localizes with NMIIA (Figure 4.2). Namely, it is possible to observe some overlapping between Arl13b tubular networks and NMIIA (Figure 4.2C and D). Lastly, there is little, if any co-localization between Arl13b and NMIIB (Figure 4.3).

Confirmation of the co-localization of actin and NMIIA or NMIIB in MDA-MB-231 cells was also performed. Indeed, actin and NMIIA co-localize in several subcellular structures, such as stress fibers, FAs and lamellipodia (Figure S1). The typical periodic pattern of alternating actin and myosin was also possible to visualize on the stress fibers of these cells (Figure S1B and D). Similarly, NMIIB co-localizes with the same type of actin cytoskeleton structures, although not as prominently as NMIIA (Figure S1C and D).

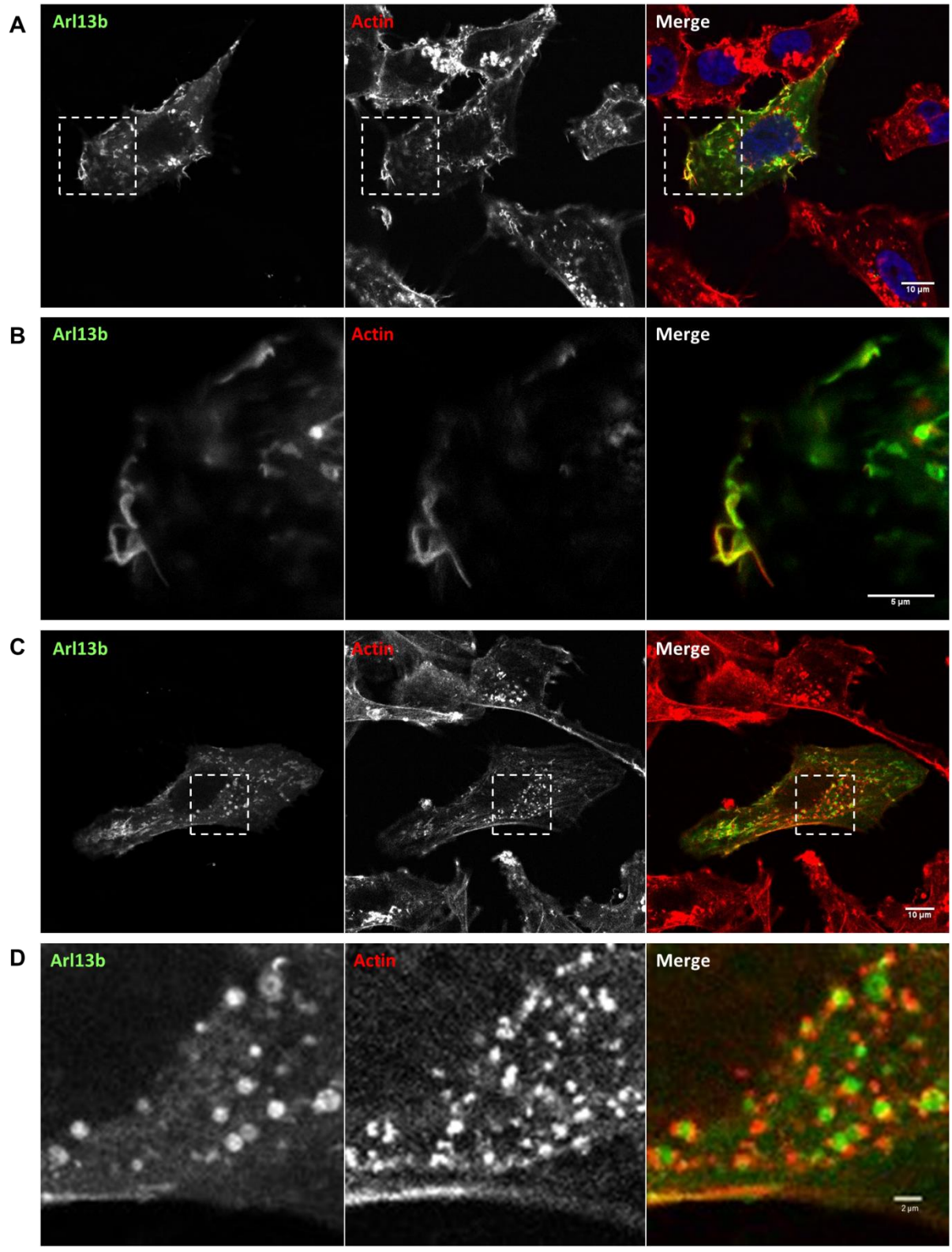

Figure 4.1 – Arl13b co-localizes with actin in MDA-MB-231 cells. MDA-MB-231 cells overexpressing Arl13b-GFP were fixed and stained with Alexa Fluor-568-conjugated phalloidin. **(A and B)** Arl13b co-localizes with actin mainly in structures localized at the cell periphery and at the plasma membrane. **(C and D)** Arl13b-positive vesicular structures are surrounded by smaller phalloidin-stained structures. B and D correspond to enlarged views of areas indicated by the boxes in A and C, respectively. All images correspond to representative Z stacks obtained by confocal microscopy. Scale bars: (A and C) 10 µm; (B) 5 µm; (D) 2 µm.

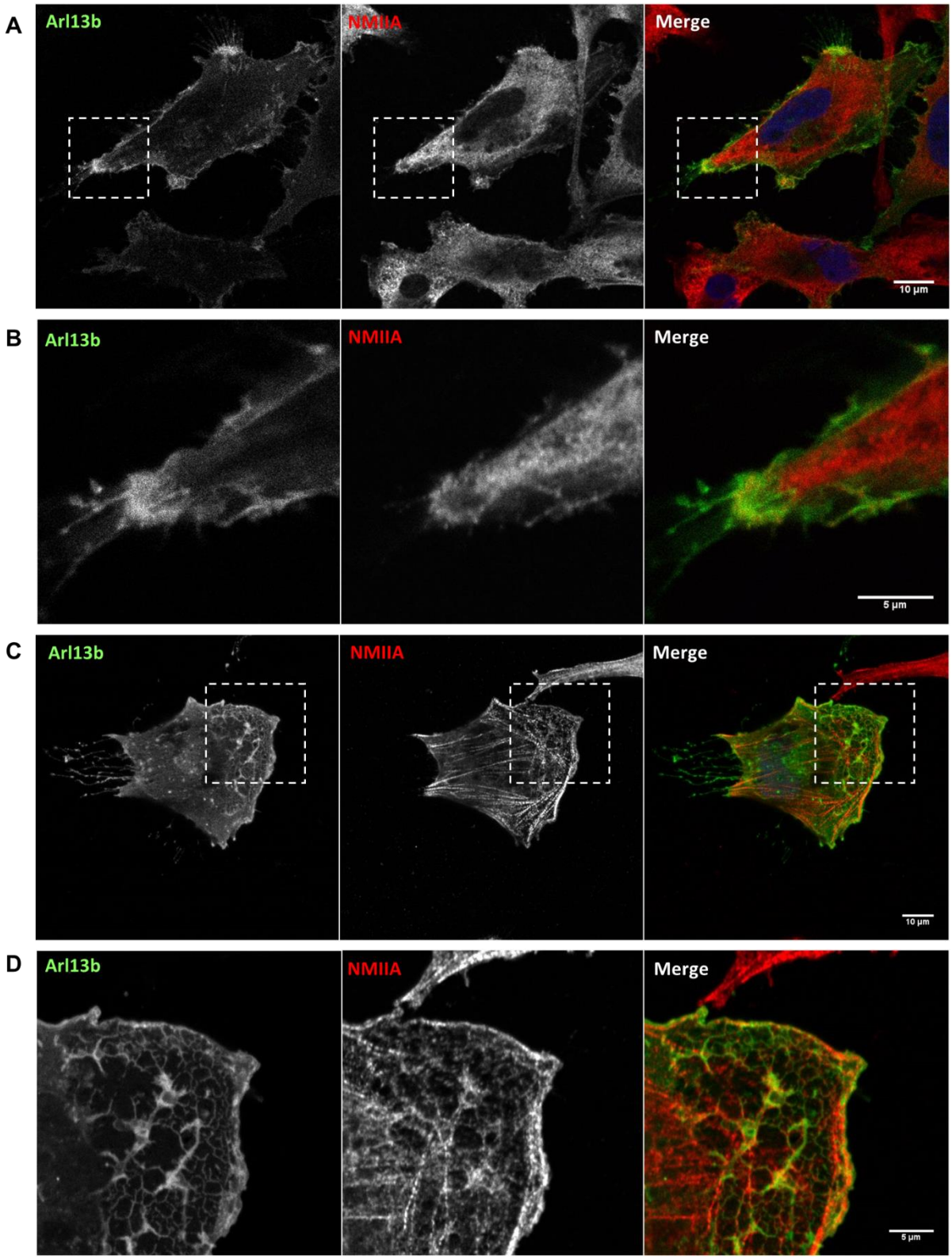

Figure 4.2 - Arl13b co-localizes with NMIIA in MDA-MB-231 cells. MDA-MB-231 cells overexpressing Arl13b-GFP were fixed and stained with anti-NMIIA antibody. **(A and B)** Arl13b co-localizes with NMIIA in a protrusive structure that resembles a CDR. Arl13b also co-localizes with NMIIA in lamellipodia. **(C and D)** Arl13b and NMIIA co-localize in the leading edge of a cell with distinctive leading (right) and trailing edges (left). Arl13b-positive tubular structures are stained and co-localize with NMIIA. B and D correspond to enlarged views of areas indicated by the boxes in A and C, respectively. All images correspond to representative Z stacks obtained by confocal microscopy. Scale bars: (A and C) 10 µm; (B and D) 5 µm.

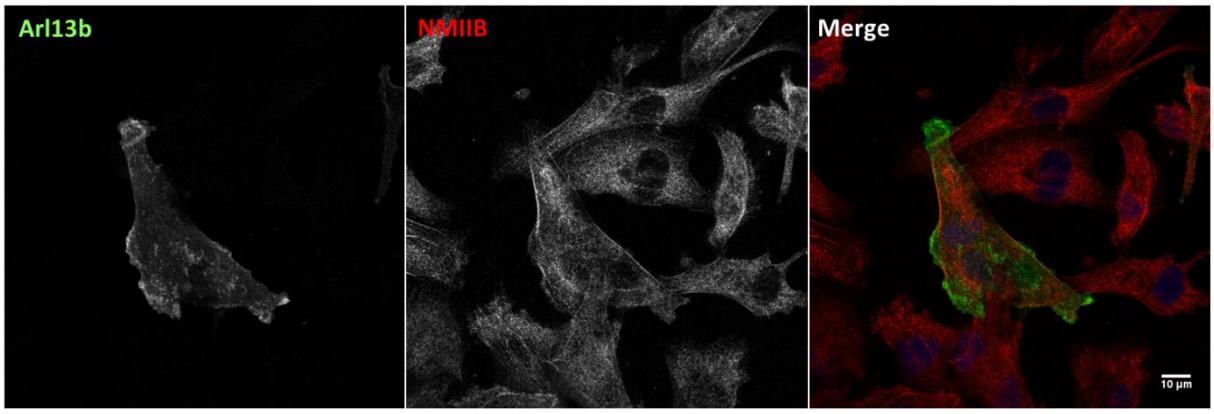

Figure 4.3 – Arl13b does not co-localize with NMIIB in MDA-MB-231 cells. MDA-MB-231 cells overexpressing Arl13b-GFP (Arl13b-GFP) were fixed and stained with anti-NMIIB antibody. The image corresponds to a representative Z stack obtained by confocal microscopy. Scale bar: 10 µm.

4.2. Interaction of Arl13b and NMIIA in non-tumorigenic and cancer breast cell lines

Recent studies from our group found evidence for an increase in Arl13b expression levels in the highly migratory and invasive MDA-MB-231 and the less migratory and invasive MCF7 breast cancer cell lines, when compared to the non-tumorigenic breast cell line MCF10A (Casalou *et al*, unpublished results). To assess if the interaction between Arl13b and NMIIA can mediate the increase in cell migration and invasion capacities, co-immunoprecipitation studies were performed with total protein extracts obtained from confluent MDA-MB-231 cells using a lysis buffer containing 1% IGEPAL. The band corresponding to NMIIA in the Arl13b immunoprecipitates was barely detectable (Figure 4.4). Nevertheless, the interaction was readily detectable when the protein extract was obtained from MDA-MB-231 cells that were previously stimulated to migrate by multiple wound scratching on a confluent monolayer. Therefore, despite the difficulty in detecting the interaction in this cell line, there is a strong interaction in migrating cells.

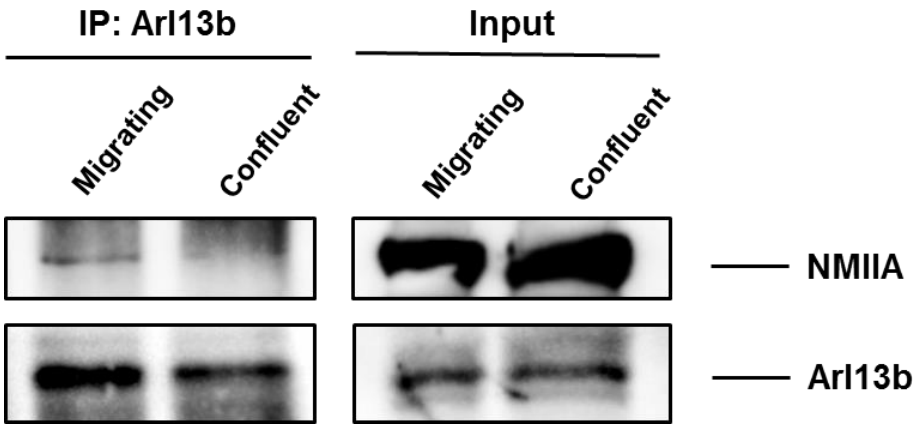

Figure 4.4 – Co-immunoprecipitation of non-muscular myosin IIA with Arl13b in MDA-MB-231 cells. MDA-MB-231 total cell extracts obtained with a lysis buffer containing 1% IGEPAL were incubated with a rabbit anti-Arl13b antibody before retrieval of the immunoprecipitates with protein G sepharose beads. The immunoprecipitated products and 40 µg of total cell extract were run on 8% SDS-PAGE. Western blot was performed with anti-NMIIA or anti-Arl13b antibodies.

In an attempt to obtain a stronger band corresponding to NMIIA in the co-immunoprecipitation experiments, MDA-MB-231 cells were transfected with plasmids encoding GFP-tagged Arl13b. This allowed a significant increase in the immunoprecipitated Arl13b and, consequently, in the co-immunoprecipitated NMIIA (Figure 4.5).

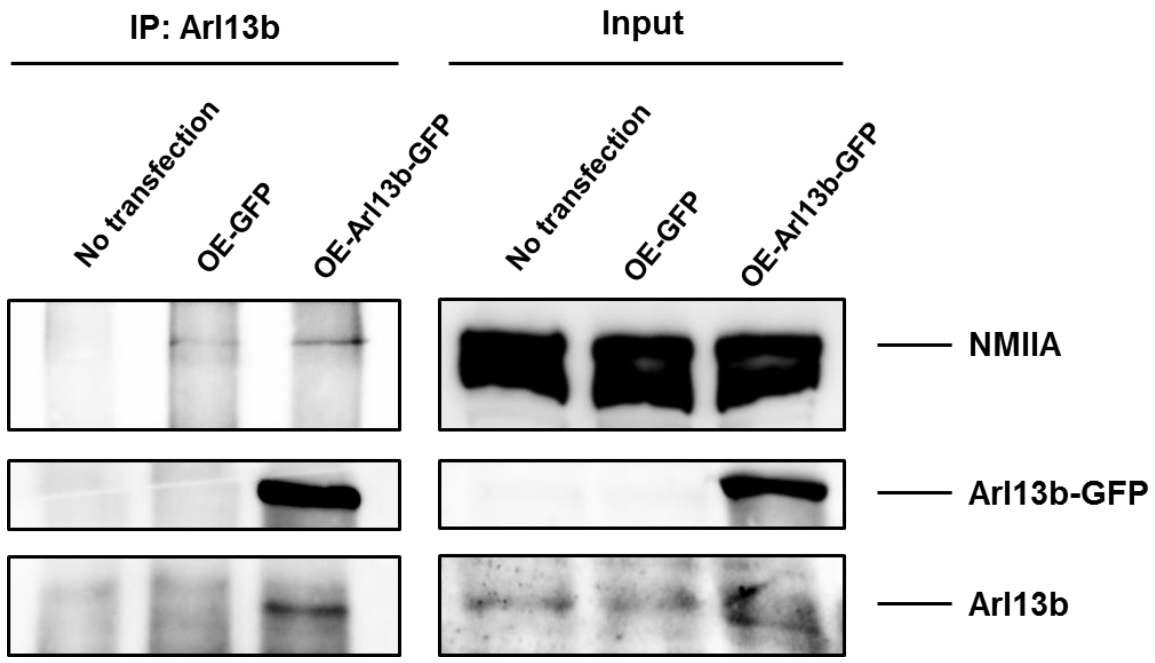

Figure 4.5 – Co-immunoprecipitation of non-muscular myosin IIA with Arl13b in MDA-MB-231 cells overexpressing Arl13b-GFP. Total cell extracts were obtained with a lysis buffer containing 1% IGEPAL from MDA-MB-231 cells which were either non-transfected, transfected with a plasmid encoding GFP or with a plasmid encoding Arl13b-GFP. Cell extracts were incubated with a rabbit anti-Arl13b antibody before retrieval of the immunoprecipitates with protein G sepharose beads. The immunoprecipitated products and 20 µg of total cell extract were run on 8% SDS-PAGE. Western blot was performed with anti-NMIIA or anti-Arl13b antibodies.

To improve the conditions of the immunoprecipitation experiments and better detect the band corresponding to NMIIA, the composition of the lysis buffer was changed by replacing IGEPAL at 1% by TX-100 (Triton X-100) at 0,1%. The reason for this was that 1% IGEPAL could be too harsh, not allowing the interaction between Arl13b and its binding partners to be preserved.

In order to compare the interaction between Arl13b and NMIIA in cell lines with different migratory and invasive capacities, Arl13b immunoprecipitation was performed in protein extracts obtained with a lysis buffer containing 0,1% TX-100 from non-tumorigenic epithelial breast cells (MCF10A), poorly invasive breast cancer cells (MCF7) and highly invasive breast cancer cells (MDA-MB-231). The use of the lysis buffer containing 0,1% TX-100 in the immunoprecipitation protocol allowed the detection of a clear band for NMIIA in all the tested cell lines (Figure 4.6). After quantification of the bands corresponding to NMIIA and Arl13b, the ratios between the signals corresponding to the NMIIA band and the Arl13b band were calculated, in order to normalize the results obtained to the amount of immunoprecipitated protein. The results suggest that NMIIA co-immunoprecipitates more with

Arl13b in MCF10A cells, followed by MCF7 and lastly by MDA-MB-231, in which there is only a faint signal. These results suggest that, despite the higher expression levels of Arl13b and NMIIA in highly migratory and invasive breast cancer cell lines (Casalou *et al*, unpublished results), the interaction between these proteins is not proportionally stronger.

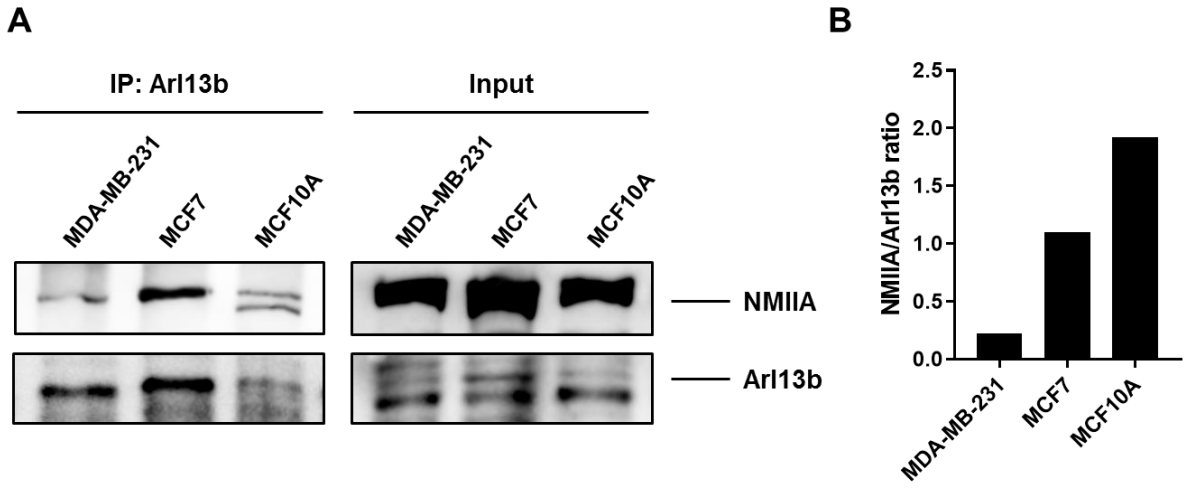

Figure 4.6 – Co-immunoprecipitation of non-muscular myosin IIA with Arl13b in distinct breast cell lines. (A) Total cell extracts were obtained from MDA-MB-231, MCF7 and MCF10A cells using a lysis buffer containing 0,1% TX-100. Cell extracts were incubated with a rabbit anti-Arl13b antibody before retrieval of the immunoprecipitates with protein G sepharose beads. The immunoprecipitated products and 20 µg of total cell extract were run on 8% SDS-PAGE. Western blot was performed with anti-NMIIA or anti-Arl13b antibodies. **(B)** The ratios between the bands corresponding to NMIIA and Arl13b were calculated to normalize the results obtained to the amount of immunoprecipitated protein. Quantification of the bands was performed using the ImageJ software.

Since Arl13b-NMIIA interaction was more clearly detected in MCF10A and MCF7 cell lines, protein extracts from these cells were used to assess the influence of a migratory stimulus on the interaction. For this end, immunoprecipitation of Arl13b was performed on protein extracts from cells that were either grown to a confluent monolayer or stimulated to migrate by making multiple wound scratches on the confluent monolayer. As previously observed, the band corresponding to NMIIA appeared stronger in the lanes corresponding to MCF10A, either in confluent or migrating conditions (Figure 4.7). Additionally, after analysis of the band ratios, it was possible to observe that there is a clear increase in co-immunoprecipitated NMIIA in migratory conditions. Moreover, this effect was verified on both cell lines but more markedly on MCF10A.

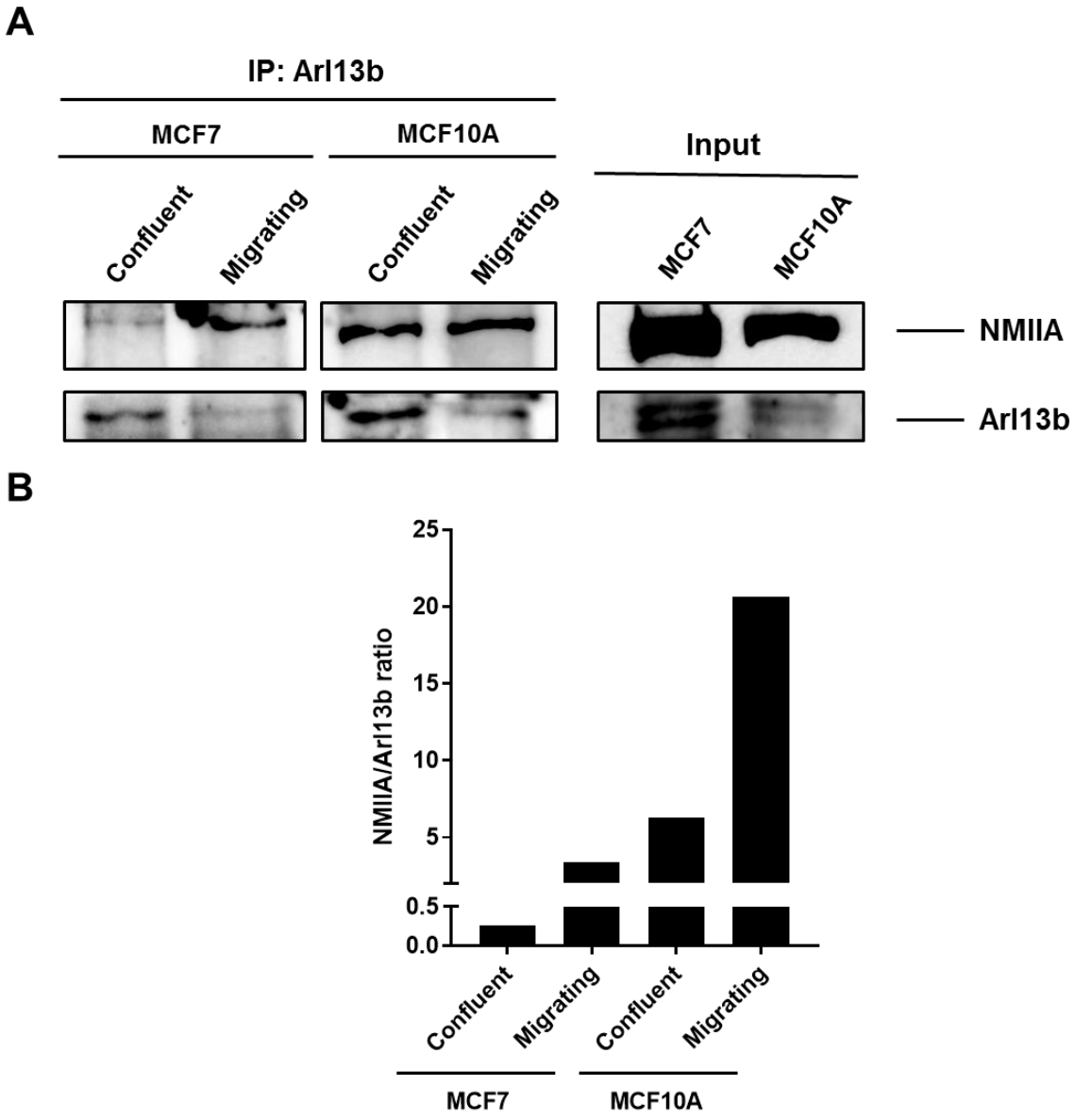

Figure 4.7 – Co-immunoprecipitation of non-muscular myosin IIA with Arl13b in MCF7 and MCF10A cells during cell migration. (A) MCF7 and MCF10A cells were either grown to a confluent monolayer or stimulated to migrate by multiple wound scratching. Total cell extracts were obtained with a lysis buffer containing 0,1% TX-100 and incubated with a rabbit anti-Arl13b antibody before retrieval of the immunoprecipitates with protein G sepharose beads. The immunoprecipitated products and 20 µg of total cell extract were run on 8% SDS-PAGE. Western blot was performed with anti-NMIIA or anti-Arl13b antibodies. **(B)** The ratios between the bands corresponding to NMIIA and Arl13b were calculated to normalize the obtained results to the amount of immunoprecipitated protein. Quantification of the bands was performed using the ImageJ software.

Our laboratory has shown that, in mouse fibroblasts, NMIIA is an Arl13b effector, interacting with its GTP-bound form. Therefore, the influence of GTP or GDP binding on the interaction between Arl13b and NMIIA interaction was assessed. To this end, MCF10A and MCF7 cell lysates were incubated with either a non-hydrolysable form of GTP (GTPɣS) or GDP (Figure 4.8). Analysis of the NMIIA band signal after normalization allowed us to conclude that loading of Arl13b with GTPɣS in

MCF10A protein extracts leads to a drastic increase in Arl13b-NMIIA interaction. On the other hand, in MCF7 protein extracts the amount of co-immunoprecipitated NMIIA was similar in both incubations with GTPγS or GDP.

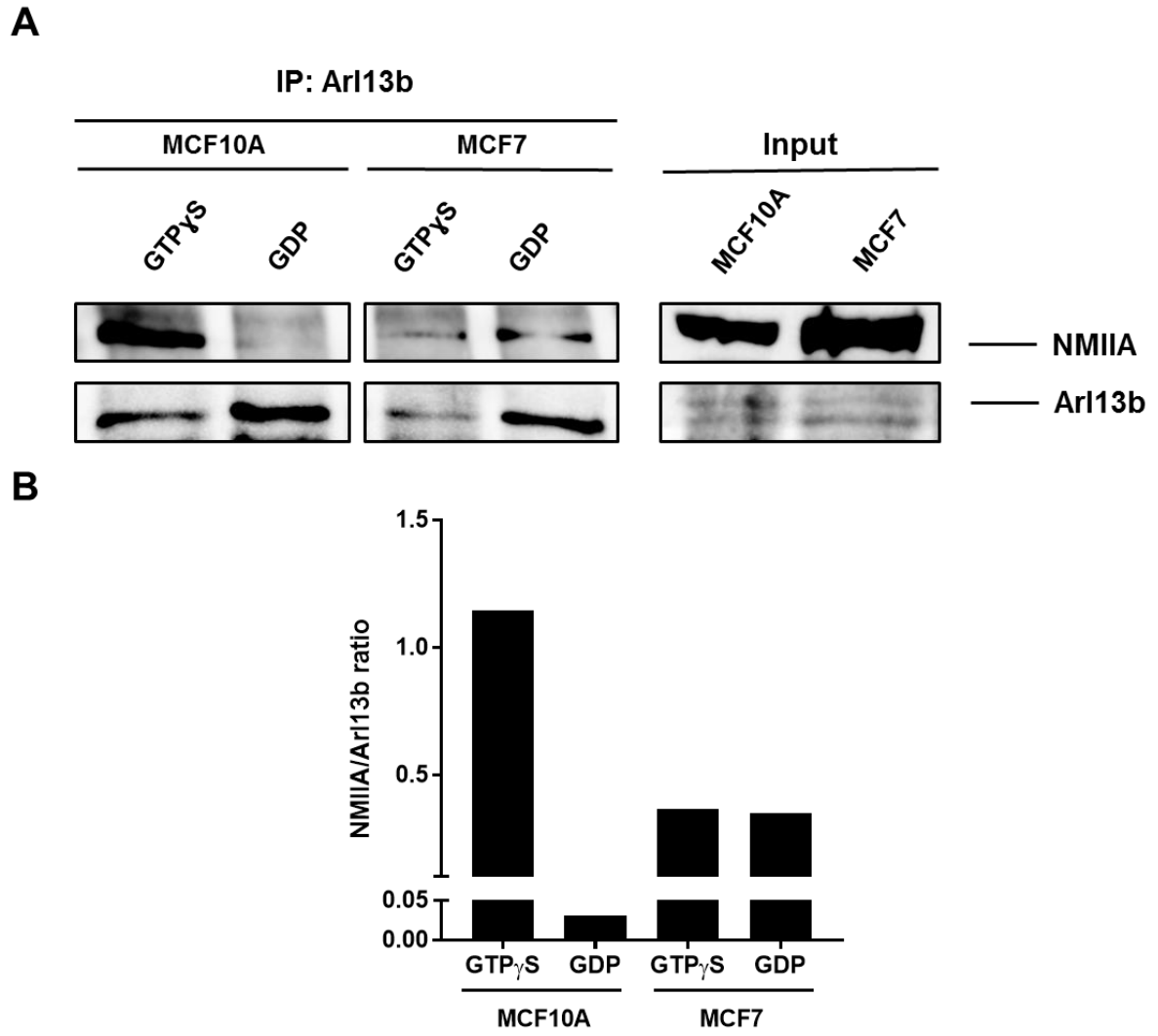

Figure 4.8 – Co-immunoprecipitation of non-muscular myosin IIA with Arl13b in GTP bound and unbound conditions. (A) Total cell extracts were obtained from MCF10A or MCF7 cells with a lysis buffer containing 0,1% TX-100 and incubated with GTPγS or GDP, before incubation with a rabbit anti-Arl13b antibody and retrieval of the immunoprecipitates with protein G sepharose beads. The immunoprecipitated products and 20 µg of total cell extract were run on 8% SDS-PAGE. Western blot was performed with anti-NMIIA or anti-Arl13b antibodies. **(B)** The ratios between the bands corresponding to NMIIA and Arl13b were calculated to normalize the obtained results to the amount of immunoprecipitated protein. Quantification of the bands was performed using the ImageJ software.

Other members of our laboratory performed immunoprecipitations using protein extracts from MCF7 cells overexpressing either Arl13b-wt-GFP or Arl13b-R79Q-GFP. Arl13b-R79Q is an Arl13b point mutant in the predicted GTP-sensitive switch 2 region, which reportedly has only approximately 50% of the GTP binding capacity of wildtype Arl13b (Cantagrel *et al*, 2008). In this case, the immunoprecipitation

of overexpressed Arl13b and its binding partners was performed using GFP-trap beads, which bind to GFP and thus allow immunoprecipitation of GFP-fusion proteins and their interacting partners.

The Arl13b-R79Q mutant was more expressed, as can be seen in the inputs, and therefore there was more protein present in the immunoprecipitates than Arl13b wildtype. Even so, the Arl13b-R79Q mutant showed less interaction with NMIIA, when comparing with Arl13b wildtype (Figure 4.9), which suggests that Arl13b GTP-binding capacity is required for Arl13b interaction with NMIIA in MCF7 cells.

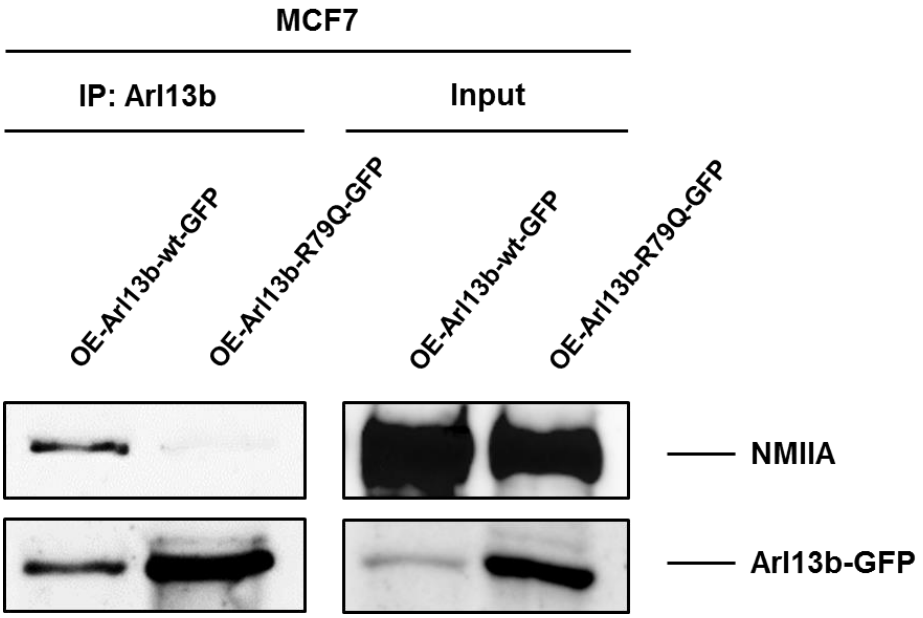

Figure 4.9 – Co-immunoprecipitation of non-muscular myosin IIA with Arl13b in MCF7 cells overexpressing Arl13b-wildtype-GFP or Arl13b-R79Q-GFP. Total cell extracts were obtained from MCF7 cells overexpressing either Arl13b-wt-GFP or Arl13b-R79Q-GFP with a lysis buffer containing 0,2% TX-100, before incubation and precipitation of GFP-tagged proteins and their interacting partners with GFP-trap beads. The immunoprecipitated products and 20 µg of total cell extract were run on 8% SDS-PAGE. Western blot was performed with anti-NMIIA or anti-GFP antibodies. Courtesy of Paul Greiner and Cristina Casalou.

4.3. Influence of NMIIA silencing on breast cancer cells migratory capacity

Our group has previously shown that the silencing of Arl13b or NMIIA in mouse fibroblasts leads to a decrease in the migratory capacity of these cells in wound healing assays (Casalou *et al*, 2014). In breast cancer cells (MCF7 and MDA-MB-231), Arl13b silencing is also associated with impaired migration and invasion in wound healing assays and transwell migration and invasion assays (Casalou *et al*, unpublished results). To test if silencing of NMIIA and/or NMIIB leads to the same phenotype, wound healing assays were performed on MCF7 and MDA-MB-231 cells after siRNA knockdown of the corresponding genes (*MYH9* and *MYH10*, respectively).

When the experiment was performed using the poorly invasive MCF7 cells, we observed that neither the silencing of NMIIA (*MYH9*), NMIIB (*MYH10*) or both lead to significant differences in the

percentage of wound closure at the different time points (Figure 4.10A). However, the depletion of these proteins on highly invasive MDA-MB-231 cells leads to a significant increase in the percentage of wound closure compared to cells transfected with a non-targeting siControl (siCtrl) at both time points (Figure 4.10). These results indicate that NMIIA and/or NMIIB silencing on MCF7 or MDA-MB-231 cell lines does not phenocopy the decreased migration that occurs upon Arl13b silencing.

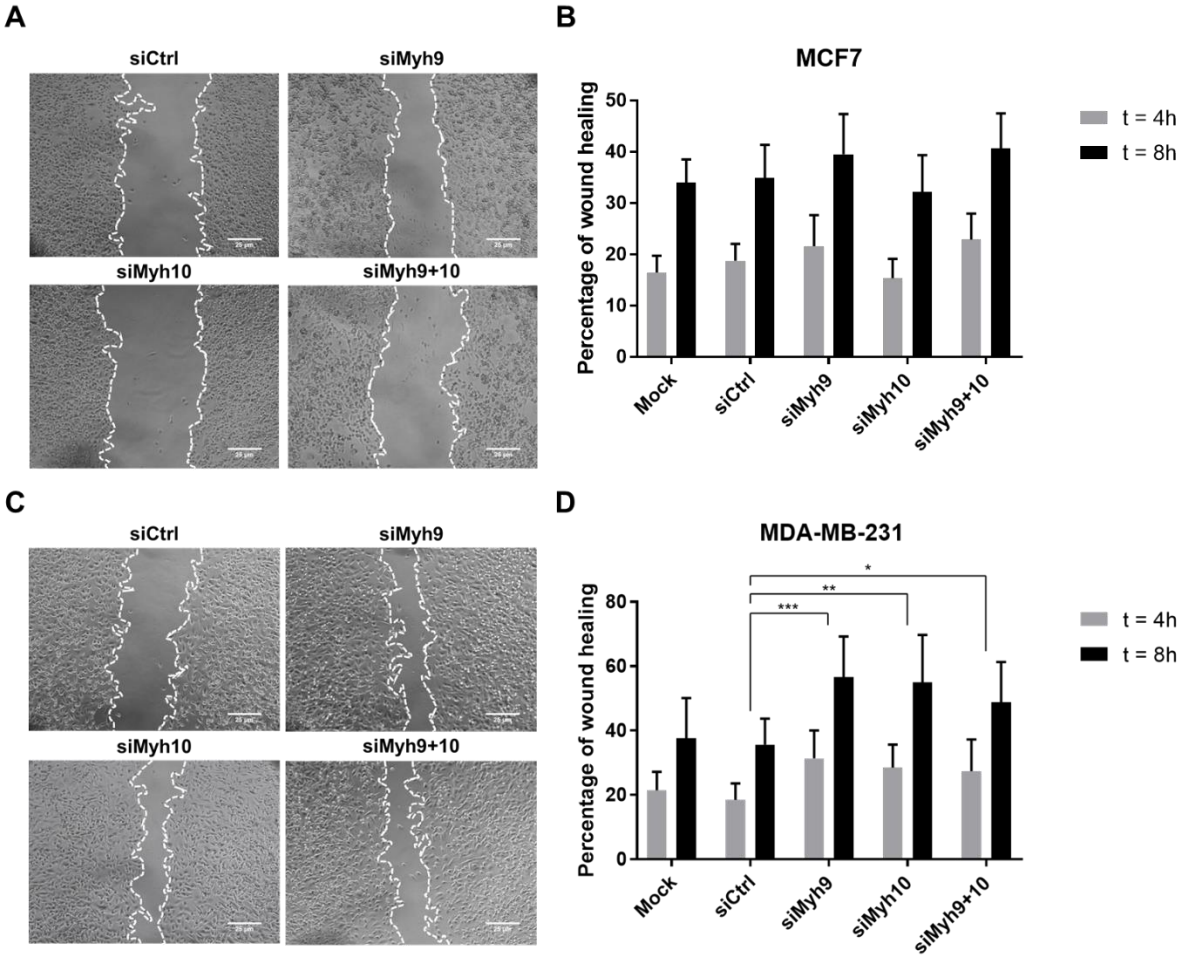

Figure 4.10 – NMIIA silencing leads to increased migration in MDA-MB-231 cells. MDA-MB-231 and MCF7 cells were silenced for NMIIA and/or NMIIB using specific siRNAs. Mock (no transfection) and siCtrl (non-targeting siRNA) were used as negative controls. Cells were grown to a confluent monolayer and a single scratch with a pipette tip was made before cell migration was induced by switching the serum-free medium to medium containing 10% FBS. The percentage of wound closure was determined by measuring the initial (t = 0h) and final (t = 4h and t = 8h) areas of the wounds. **(A and C)** Representative images of the wound closure 8 hours after the wound scratching (t = 8h) on MCF7 (A) and MDA-MB-231 (C) confluent monolayers. Scale bars: 25 µm. **(B and D)** Percentage of wound closure 4 hours and 8 hours after the wound scratching on MCF7 (B) and MDA-MB-231 (D) confluent monolayers. Results represent mean ± standard deviation. *P<0.05; **P<0.005; ***P<0.001 (One-way ANOVA with Dunnett's multiple comparisons test).

Silencing of *MYH9* and *MYH10* genes was confirmed by analysis of mRNA levels through real-time quantitative PCR (RT-qPCR) (Figure S2). In MCF7 cells, there was an average of 81,93% of mRNA silencing for the *MYH9* gene and 77,24% for the *MYH10* gene (Figure S2A and B). In MDA-MB-231 cells, the average was of 83,34% for *MYH9* and 85,22% for *MYH10* (Figure S2C and D). In the case of

MDA-MB-231 cells, confirmation of NMIIA and NMIIB protein silencing was obtained by Western blotting (Figure S3).

4.4. Identification of candidate Arl13b interacting partners that can mediate Arl13b function on cell migration

With the aim of identifying Arl13b-binding partners that could be involved in the function of Arl13b in cell migration, Arl13b immunoprecipitation was performed in protein extracts from MCF10A or MDA-MB-231 cells that were either grown to a confluent monolayer or stimulated to migrate by making multiple wound scratches on a confluent monolayer. Since this was performed before changing the lysis buffer composition, a lysis buffer containing 0,1% IGEPAL was used for this experiment. After SDS-PAGE, Coomassie Briliant Blue G-250 staining followed by silver nitrate staining were performed to detect Arl13b co-immunoprecipitating proteins on the preparative gel. Upon comparison of migrating and confluent conditions, protein bands that appeared on one of the conditions and not on the other, as well as bands that had significant differences in intensity, were excised. After excision and tryptic band digestion, mass spectrometry was performed in order to identify the proteins. Proteins which were identified with high confidence levels are presented on Table 4.1. Before the preparative gel, from which the bands were excised for mass spectrometry analysis, an analytical gel was obtained with co-immunoprecipitates from MDA-MB-231 cell extracts using the same experimental procedures (Figure 4.11A).

Table 4.1 – Mass spectrometry identification of Arl13b-interacting partners that can be involved in Arl13b function in cell migration. Proteins from migrating or confluent MCF10A and MDA-MB-231 cell extracts that co-immunoprecipitated with Arl13b were run on SDS-PAGE before gel staining. Upon comparison of migrating and confluent conditions, protein bands that appeared on one condition and not the other or had differences in intensity were excised. After tryptic digestion, proteins were identified by Mass Spectrometry. Unused ProtScore reflect confidence levels of the protein identification. Selected proteins with Unused ProtScore values over 2.0 (identification confidence of 99%) are listed, as well as respective Unused ProtScores.

Protein	**Unused ProtScore**
Actin	45.69
Annexin A2	3.11
Desmoglein-1	2.23
Desmoplakin	6.9
Erlin-1	4.77
Erlin-2	22.34
Hornerin	4.16
NMIIA	15.54
Protein S100-A8	2.0
Tropomodulin-1	4.57
Tropomodulin-3	13.36

Actin and NMIIA, which were already shown to interact with Arl13b (Barral *et al*, 2012; Casalou *et al*, 2014), were identified with high confidence levels.

Both Erlin-1 and Erlin-2, which are associated with the regulation of cellular cholesterol homeostasis, were also identified with high confidence levels. It is interesting to note that several other proteins related with lipid metabolism and transport were identified as Arl13b-binding partners, such as Annexin A2.

Other proteins, associated with the dynamics of cytoskeleton and adhesion, such as tropomodulins, Desmoplakin, Desmoglein-1, Hornerin and Protein S100-A8, were also identified. This is in agreement with the known interaction of Arl13b with actin and NMIIA. Interestingly, Hornerin and Protein S100-A8, members of the S100 protein family, have already been associated with breast cancer and tumor progression (Fleming *et al*, 2012).

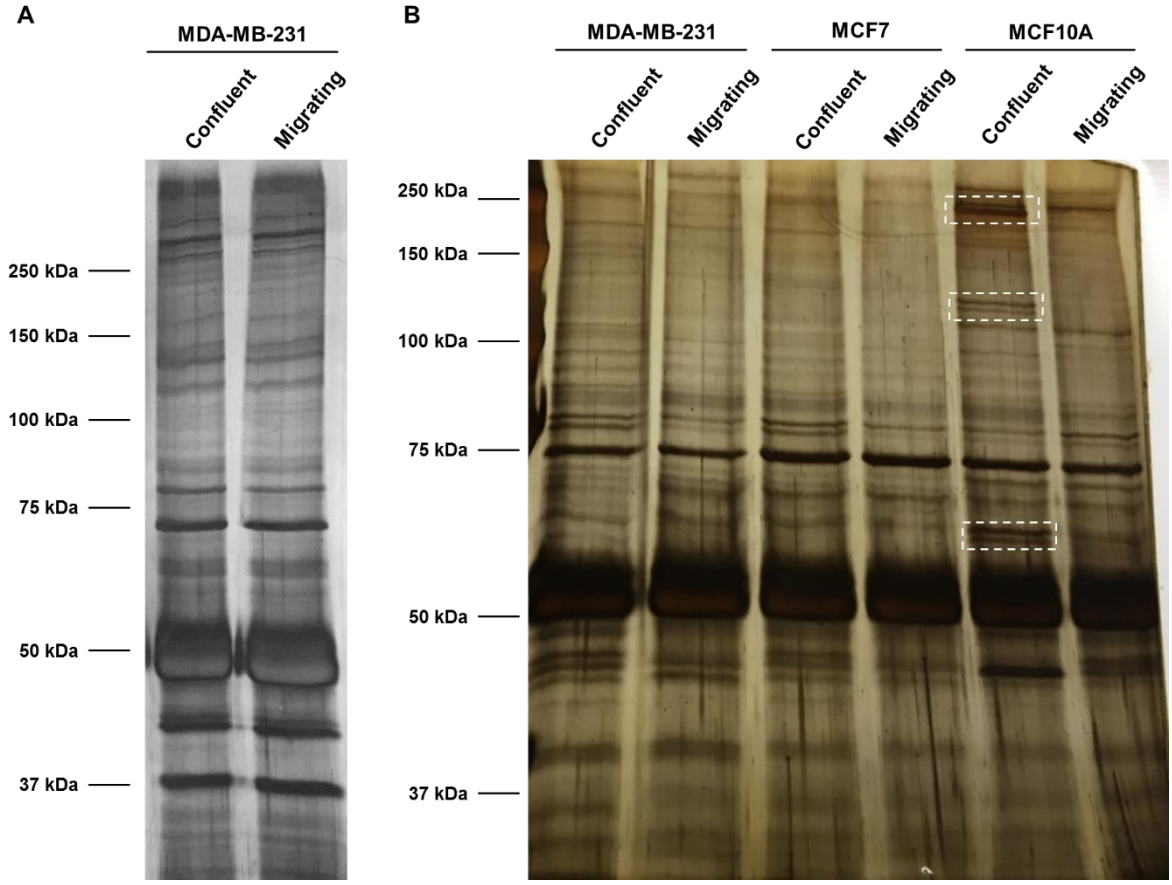

Figure 4.11 – Silver nitrate staining of gels loaded with Arl13b co-immunoprecipitates. (A) Analytical gel loaded with Arl13b interacting partners from MDA-MB-231 cells. **(B)** Preparative gel loaded with Arl13b interacting partners from MDA-MB-231, MCF7 and MCF10A cells. MDA-MB-231, MCF7 and MCF10A cells were either grown to a confluent monolayer or stimulated to migrate by multiple wound scratching. Total cell extracts were obtained with a lysis buffer containing either 1% IGEPAL (A) or 0,1% TX-100 (B) and incubated with a rabbit anti-Arl13b antibody before retrieval of the immunoprecipitates with protein G sepharose beads. The immunoprecipitated products were run on 8% SDS-PAGE and the gel was stained with Coomassie Briliant Blue G-250 (A) or R-250 (B) followed by silver nitrate staining. Indicated sections correspond to examples of bands that, when comparing migrating and confluent conditions in the same cell line, are present on one condition and not the other or have different intensities, and therefore are considered candidates to mediate Arl13b function in breast cancer cell migration.

Since replacing 1% IGEPAL for 0,1% TX-100 in the lysis buffer composition allowed a clearer detection of NMIIA co-immunoprecipitating with Arl13b (section 4.2), we hypothesized that it would also improve the detection of other Arl13b-interacting partners. Thus, an analytical gel was loaded with Arl13b immunoprecipitates from protein extracts obtained from MDA-MB-231, MCF7 and MCF10A cells in confluent or migrating conditions using a lysis buffer containing 0,1% TX-100. As before, any bands present in one condition and not the other or that have different intensities in different conditions are considered relevant for our goal of identifying Arl13b-interacting partners important for Arl13b function in breast cancer cell migration. Silver nitrate staining allowed the detection of some differences between confluent and migratory conditions and even between the distinct cell lines analyzed (Figure 4.11B). Interestingly, the most pronounced differences were found between the lanes corresponding to confluent and migrating MCF10A cells.

5. Discussion

Previous results from our group showed that the small G protein Arl13b plays a role in cell migration of mouse fibroblasts, as well as in both highly migratory and invasive MDA-MB-231 and poorly invasive MCF7 breast cancer cells (Casalou *et al*, 2014; Casalou *et al*, unpublished results). In mouse fibroblasts, it was also shown that NMIIA is an Arl13b effector and mediates its functions on cell migration (Casalou *et al*, 2014). Therefore, we proposed to study the mechanism by which Arl13b regulates the migration of breast cancer cells and more specifically the role of NMIIA in mediating this process.

Since in mouse fibroblasts Arl13b co-localizes with actin and NMIIA (Barral *et al*, 2012; Casalou *et al*, 2014), we started by confirming this co-localization in MDA-MB-231 cells. In fact, it was possible to detect co-localization between Arl13b and actin, as well as NMIIA, mainly in structures associated with cell migration at the cell periphery. Additionally, it was possible to observe Arl13b-positive vesicles associated with the actin cytoskeleton. These observations suggest that the association of Arl13b with the actin cytoskeleton and NMIIA is conserved in MDA-MB-231 cells. On the other hand, no co-localization between Arl13b and NMIIB could be detected, which indicates that Arl13b and NMIIB, and consequently NMIIA and NMIIB, have different subcellular localization.

The interaction between Arl13b and NMIIA was confirmed by co-immunoprecipitation studies. Considering the highly migratory and invasive capacities of MDA-MB-231 cells and that NMIIA is an Arl13b effector associated with its functions in cell migration (Casalou *et al*, 2014), we expected to observe a strong interaction between these proteins. However, when the immunoprecipitation was performed using MDA-MB-231 cell extracts obtained with a lysis buffer containing 1% IGEPAL, the band corresponding to NMIIA was hardly detectable. Nevertheless, using the same experimental conditions, we clearly detected NMIIA co-immunoprecipitating with Arl13b in cell extracts from migrating MDA-MB-231 cells, which suggests that the interaction between Arl13b and NMIIA is stronger during cell migration. Furthermore, the use of MDA-MB-231 cells overexpressing Arl13b-GFP also allowed us to confirm the Arl13b-NMIIA interaction in MDA-MB-231 cells.

We further optimized the immunoprecipitation protocol by replacing IGEPAL at 1% for TX-100 at 0,1% in the lysis buffer composition. This change resulted in a significant increase in the signal strength of the NMIIA band after Arl13b immunoprecipitation in all the tested cell lines. Presumably, the lower concentration of detergent lowered the stringency from the immunoprecipitation reactions, allowing a better preservation of the interactions between Arl13b and its binding partners and consequently the strengthening of the signal of the co-immunoprecitating proteins.

After this change in the lysis buffer composition, the influence of different factors on Arl13b-NMIIA interaction was assessed, namely the different migratory capacities of distinct breast cell lines, migrating *versus* confluent conditions of the cells and the presence of an excess of GTPɣS or GDP. Surprisingly, analysis of co-immunoprecitated NMIIA after normalization of the results suggests that there is a stronger Arl13b-NMIIA interaction in non-tumorigenic MCF10A breast cells, followed by

the poorly invasive MCF7 cells and finally by the highly invasive MDA-MB-231 cells. Furthermore, co-immunoprecipitation studies using MCF7 and MCF10A cells suggest that, in both cell lines, the interaction between Arl13b and NMIIA is stronger when cells are migrating, as had already been observed in the MDA-MB-231 cell line in this study and in mouse fibroblasts (Casalou *et al*, 2014). Finally, Arl13b binding to GTPɣS leads to a dramatic increase in Arl13b-NMIIA interaction in MCF10A cells when comparing with binding to GDP, while the same was not observed in MCF7 cells. However, other studies from our group using MCF7 cells showed that the interaction of GTP-binding-deficient Arl13b-R79Q mutant with NMIIA was markedly reduced when comparing to wildtype Arl13b, even with higher amount of immunoprecipitated Arl13b-R79Q than wildtype Arl13b. This supports the idea that Arl13b GTP-binding capacity is required for Arl13b-NMIIA interaction in MCF7 cells. Therefore, considering that overall these results and previous studies (Casalou *et al*, 2014) indicate that the Arl13b-NMIIA interaction depends on Arl13b binding to GTP, the lack of differences in co-immunoprecipitated NMIIA upon GTPɣS or GDP loading in MCF7 cell extracts, which was observed in a single co-immunoprecipitation experiment (Figure 4.8), may be associated with technical problems and has to be further explored.

Altogether, the co-immunoprecipitation results suggest that the overall characteristics of the Arl13b-NMIIA interaction are maintained in the different breast cell lines, since in all of them the binding of Arl13b to its effector NMIIA seems to be stronger in migrating cells and dependent on Arl13b activation. However, our results also suggest that MCF10A, MCF7 and MDA-MB-231 cells regulate cell migration through different molecular mechanisms, which are characterized by distinct levels of NMIIA-dependency. This can be understood in the context of cancer cell progression, considering that the accumulation of mutations in cancer cells leads to adaptations in their migratory capacities (Hanahan and Weinberg, 2011). As such, Arl13b-NMIIA interaction seems to be more important for the migration of cells will slow motility such as MCF10A and less important in fast-migrating cells such as MCF7 and MDA-MB-231. These results are corroborated by our observations which showed that mouse fibroblasts depend on NMIIA to migrate (Casalou *et al*, 2014).

In fact, NMIIA silencing in MCF7 cells does not lead to significant changes in the speed of wound closure on wound healing assays and in MDA-MB-231 cells leads to an increase in cell migration. This further suggests that NMIIA has different roles in the studied cell lines, characterized by distinct migratory capacities. While silencing of NMIIA leads to a decrease in cell migration of mouse fibroblasts, mimicking the phenotype of Arl13b silencing in these cells (Casalou *et al*, 2014), silencing of NMIIA in MCF7 and MDA-MB-231 cells does not phenocopy the decrease in cell migration that also occurs upon Arl13b silencing in these cells (Casalou *et al*, unpublished results). Presumably, NMIIA silencing in slow-migrating MCF10A cells could lead to a decrease in cell migration, which could be confirmed by future wound healing experiments.

We also found that NMIIB silencing has similar effects to the silencing of NMIIA in the wound healing assay, indicating redundancy of the functions of the two NMII isoforms in cell migration. Since

the silencing of both NMII isoforms does not exacerbate the enhancement of cell migration, this hypothesis is further strengthened. This is consistent with the fact that NMIIA and NMIIB both contribute to the generation of contraction forces that lead to the traction of the migrating cell body, even though the NMIIA functions are generally associated to the cell's leading edge and NMIIB is generally associated to the cell's trailing edge (Vicente-Manzanares *et al*, 2009).

Given the tumorigenic and highly migratory and invasive properties of MDA-MB-231 cells, they most likely have undergone multiple mutagenic events during cancer cell progression, which led to changes on the mechanisms of cell migration used by these cells. Thus, although MCF10A, MCF7 and MDA-MB-231 all have epithelial origin (Soule *et al*., 1973, 1990; Cailleau *et al.*, 1974), the mechanisms of cell migration of the highly invasive and migratory MDA-MB-231 breast cancer cells are presumably different from those of the non-tumorigenic MCF10A breast cells, as well as from those of the poorly invasive MCF7 breast cancer cells. In fact, as mentioned in the Introduction, it has been reported that slow-migrating cells seem to be more dependent on NMII to migrate, since their motility is based on the formation of mature adhesion structures and stress fibers, which are both NMII-dependent (Vicente-Manzanares *et al*, 2009). On the other hand, fast-migrating cells seem less dependent on NMII activation, since their rapid adhesion turnover and actin polymerization make cell migration possible without the need of actomyosin contraction to generate traction forces and slow down the retrograde flow, respectively (Vicente-Manzanares *et al*, 2009). Being this the case, while in MCF10A NMIIA silencing leads to loss of the actomyosin contractile forces needed for slow migration, in MDA-MB-231 NMIIA silencing may facilitate their fast migration.

Even so, it is important to consider that distinct mechanisms are responsible for two-dimensional and three-dimensional cell migration (Jorrisch *et al*, 2013). While two-dimensional migration may be possible without considerable traction forces and the absence of distinctive adhesion structures, this may not be the case for the more physiological three-dimensional cell migration (Jorrisch *et al.*, 2013), in which NMII-generated forces can be essential. Thus, NMII silencing could have a different impact on the speed of migration of MDA-MB-231 or MCF7 cells *in vivo* and could eventually lead to an impairment in the process.

Since the ultimate goal of this study was to unravel the molecular mechanisms of Arl13b function on cell migration, we set out to identify other proteins that can be relevant Arl13b-interacting partners in this context. By comparing proteins that co-immunoprecipitate with Arl13b in migrating or confluent conditions using MCF10A or MDA-MB-231 cell extracts, proteins that were present in one condition and not in the other or that had significant differences in intensity were identified by mass spectrometry. Actin and NMIIA, which were already known Arl13b-binding proteins (Barral *et al*, 2012; Casalou *et al*, 2014), were identified with high confidence levels, as expected. In agreement with the interaction with actin and NMIIA, other proteins associated with the cytoskeleton dynamics and adhesion were also identified. These may be involved in the molecular pathways associated with Arl13b during cell migration. Among these candidates, Hornerin and Protein S100-A8 are interesting to explore further, since there are

already reported links between these proteins and breast cancer and tumor progression (Fleming *et al*, 2012). Interestingly, several proteins associated with lipid metabolism and transport, such as Erlin-1, Erlin-2 and Annexin A2 have also been identified. Although none of these candidates have any known links to cell migration, these results may point to some other new physiological functions of Arl13b.

Similar to what occurred in the co-immunoprecipitation experiments, the use of a lysis buffer containing 0,1% TX-100 allowed a better detection of differences between the lanes corresponding to migrating and confluent conditions, as well as even between lanes corresponding to different cell lines. Particularly in the MCF10A samples, it was possible to detect pronounced differences between the lanes corresponding to migrating and confluent conditions. Using these experimental conditions, a new mass spectrometry analysis could identify additional Arl13b-interacting proteins that may be relevant for the role of Arl13b in cell migration.

With this study, novel insights on the requirement of the interaction between Arl13b and NMIIA for breast cancer cell migration were acquired, confirming that in these cells this interaction is increased in migrating conditions and dependent on Arl13b activation. However, due to distinct NMIIA functions in breast cells with different migratory capacities, Arl13b-NMIIA interaction was found to be more important for the motility of the non-tumorigenic MCF10A cells than the motility of MCF7 or MDA-MB-231 breast cancer cells. Consequently, although in MCF7 and MDA-MB-231 cells NMIIA interaction with Arl13b is associated with cell migration and NMIIA has increased levels of expression (Casalou *et al*, unpublished results), the enhanced migratory capacities that result of increased Arl13b expression are not explained by a similar increase in interaction with its effector NMIIA. As such, it is important to identify other Arl13b-interacting partners, such as effectors, GAPs or GEFs, in order to understand how Arl13b regulates cell migration in cancer cells. Specifically, further studies considering the already identified or new candidate proteins could contribute to the unravelling of the molecular mechanisms of breast cancer cell migration and to the identification of new targets for the development of anti-cancer therapies.

References

Abercrombie, M., Joan, E., Heaysman, M., and Pegrum, S. M., 1970. The locomotion of fibroblasts in culture. II. “Ruffling.” Experimental Cell Research 60(3): 437–444.

Barral, D. C., Garg, S., Casalou, C., Watts, G. F. M., Sandoval, J. L., Ramalho, J. S., Hsu, V. W., and Brenner, M. B., 2012. Arl13b regulates endocytic recycling traffic. Proceedings of the National Academy of Sciences of the United States of America 109(52): 21354–21359.

Bernards, A., and Settleman, J., 2004. GAP control: Regulating the regulators of small GTPases. Trends in Cell Biology. 14(7): 377–385.

Betapudi, V., Licate, L. S., and Egelhoff, T. T., 2006. Distinct roles of nonmuscle myosin II isoforms in the regulation of MDA-MB-231 breast cancer cell spreading and migration. Cancer Research 66(9): 4725–4733.

Buccione, R., Orth, J. D., and McNiven, M. A., 2004. Foot and mouth: podosomes, invadopodia and circular dorsal ruffles. Nature Reviews Molecular Cell Biology 5(8): 647–657.

Burridge, K., and Guilluy, C., 2016. Focal adhesions, stress fibers and mechanical tension. Experimental Cell Research. 343(1): 14–20.

Cailleau, R., Young, R., Olivé, M., and Reeves, W. J., 1974. Breast tumor cell lines from pleural effusions. Journal of the National Cancer Institute 53(3): 661–674.

Cantagrel, V., Silhavy, J. L., Bielas, S. L., Swistun, D., Marsh, S. E., Bertrand, J. Y., Audollent, S., Attié-Bitach, T., Holden, K. R., Dobyns, W. B., Traver, D., Al-Gazali, L., Ali, B. R., Lindner, T. H., Caspary, T., Otto, E. A., Hildebrandt, F., Glass, I. A., Logan, C. V., Johnson, C. A., Bennett, C., Brancati, F., Valente, E. M., Woods, C. G., and Gleeson, J. G., 2008. Mutations in the Cilia Gene ARL13B Lead to the Classical Form of Joubert Syndrome. American Journal of Human Genetics 83(2): 170–179.

Carvalho, A. T. P., Szeler, K., Vavitsas, K., Åqvist, J., and Kamerlin, S. C. L., 2015. Modeling the mechanisms of biological GTP hydrolysis. Archives of Biochemistry and Biophysics 582 80–90.

Casalou, C., Faustino, A., and Barral, D. C., 2016. Arf proteins in cancer cell migration. Small GTPases Taylor & Francis 7(4): 270–282.

Casalou, C., Seixas, C., Portelinha, A., Pintado, P., Barros, M., Ramalho, J. S., Lopes, S. S., and Barral, D. C., 2014. Arl13b and the non-muscle myosin heavy chain IIA are required for circular dorsal ruffle formation and cell migration. Journal of Cell Science 127(12): 2709–2722.

Case, L. B., and Waterman, C. M., 2015. Integration of actin dynamics and cell adhesion by a three-dimensional, mechanosensitive molecular clutch. Nature Cell Biology 17(8): 955–963.

Caspary, T., Larkins, C. E., and Anderson, K. V., 2007. The Graded Response to Sonic

Hedgehog Depends on Cilia Architecture. Developmental Cell 12(5): 767–778.

Chen, P. W., Jian, X., Heissler, S. M., Le, K., Luo, R., Jenkins, L. M., Nagy, A., Moss, J., Sellers, J. R., and Randazzo, P. A., 2016. The Arf GTPase-activating protein, ASAP1, binds nonmuscle myosin 2A to control remodeling of the actomyosin network. Journal of Biological Chemistry 291(14): 7517–7526.

Cherfils, J., and Zeghouf, M., 2013. Regulation of Small GTPases by GEFs, GAPs, and GDIs. Physiological Reviews 93(1): 269–309.

Chhabra, E. S., and Higgs, H. N., 2007. The many faces of actin: matching assembly factors with cellular structures. Nature cell biology 9(10): 1110–1121.

Choi, C. K., Vicente-Manzanares, M., Zareno, J., Whitmore, L. A., Mogilner, A., and Horwitz, A. R., 2008. Actin and α-actinin orchestrate the assembly and maturation of nascent adhesions in a myosin II motor-independent manner. Nature Cell Biology 10(9): 1039–1050.

Combedazou, A., Choesmel-Cadamuro, V., Gay, G., Liu, J., Dupre, L., Ramel, D., and Wang, X., 2016. Myosin II governs collective cell migration behaviour downstream of guidance receptor signalling. Journal of Cell Science 1–7.

Donaldson, J. G., and Jackson, C. L., 2011. ARF family G proteins and their regulators: roles in membrane transport, development and disease. Nature Reviews Molecular Cell Biology Nature Publishing Group 12(6): 362–375.

Doyle, A. D., Kutys, M. L., Conti, M. A., Matsumoto, K., Adelstein, R. S., and Yamada, K. M., 2012. Micro-environmental control of cell migration--myosin IIA is required for efficient migration in fibrillar environments through control of cell adhesion dynamics. Journal of cell science 125(Pt 9): 2244–2256.

Even-Ram, S., Doyle, A. D., Conti, M. A., Matsumoto, K., Adelstein, R. S., and Yamada, K. M., 2007. Myosin IIA regulates cell motility and actomyosin-microtubule crosstalk. Nature Cell Biology 9(3): 299–309.

Fife, C. M., McCarroll, J. A., and Kavallaris, M., 2014. Movers and shakers: Cell cytoskeleton in cancer metastasis. British Journal of Pharmacology 171(24): 5507–5523.

Firat-karalar, E. N., and Welch, M. D., 2012. New mechanisms and functions of actin nucleation. Current Opinion in Cell Biology 23(1): 4–13.

Fleming, J. M., Ginsburg, E., Oliver, S. D., Goldsmith, P., and Vonderhaar, B. K., 2012. Hornerin, an S100 family protein, is functional in breast cells and aberrantly expressed in breast cancer. BMC Cancer 12(1): 266.

Friedl, P., 2004. Prespecification and plasticity: Shifting mechanisms of cell migration. Current

Opinion in Cell Biology. 16(1): 14–23.

Friedl, P., Locker, J., Sahai, E., and Segall, J. E., 2012. Classifying collective cancer cell invasion. Nature Cell Biology 14(8): 777–783.

Gaggioli, C., Hooper, S., Hidalgo-Carcedo, C., Grosse, R., Marshall, J. F., Harrington, K., and Sahai, E., 2007. Fibroblast-led collective invasion of carcinoma cells with differing roles for RhoGTPases in leading and following cells. Nature Cell Biology 9(12): 1392–1400.

Gardel, M. L., Schneider, I. C., Aratyn-Schaus, Y., and Waterman, C. M., 2010. Mechanical Integration of Actin and Adhesion Dynamics in Cell Migration. Annual Review of Cell and Developmental Biology 26(1): 315–333.

Geiger, B., Bershadsky, A., Pankov, R., Yamada, K. M., and Correspondence, B. G., 2001. Transmembrane extracellular matrix– cytoskeleton crosstalk. Nature reviews. Molecular cell biology 2(November): 793–805.

Goitre, L., Trapani, E., Trabalzini, L., and Retta, S. F., 2014. The ras superfamily of small GTPases: The unlocked secrets. Methods in Molecular Biology. 1120 1–18.

Gotthardt, K., Lokaj, M., Koerner, C., Falk, N., Gießl, A., and Wittinghofer, A., 2015. A G-protein activation cascade from Arl13B to Arl3 and implications for ciliary targeting of lipidated proteins. eLife 4(NOVEMBER2015):

Gu, Z., Noss, E. H., Hsu, V. W., and Brenner, M. B., 2011. Integrins traffic rapidly via circular dorsal ruffles and macropinocytosis during stimulated cell migration. Journal of Cell Biology 193(1): 61–70.

Hanahan, D., and Weinberg, R. A., 2011. Hallmarks of cancer: The next generation. Cell Elsevier Inc. 144(5): 646–674.

Heasman, S. J., and Ridley, A. J., 2008. Mammalian Rho GTPases: new insights into their functions from in vivo studies. Nature Reviews Molecular Cell Biology 9(9): 690–701.

Herrmann, C., 2003. Ras-effector interactions: After one decade. Current Opinion in Structural Biology. 13(1): 122–129.

Hoon, J.-L., Wong, W.-K., and Koh, C.-G., 2012. Functions and regulation of circular dorsal ruffles. Molecular and cellular biology 32(21): 4246–4257.

Itoh, T., and Hasegawa, J., 2013. Mechanistic insights into the regulation of circular dorsal ruffle formation. Journal of Biochemistry. 153(1): 21–29.

Ivanova, A. A., Caspary, T., Seyfried, N., Duong, D., West, A. B., Liu, Z., and Kahn, R. A., 2017. Biochemical characterization of purified, recombinant murine ARL13B as an atypical GTPase and ARL3 guanine nucleotide exchange factor (GEF). Journal of Biological Chemistry 1–36.

Jorrisch, M. H., Shih, W., and Yamada, S., 2013. Myosin IIA deficient cells migrate efficiently despite reduced traction forces at cell periphery. Biology open 2(4): 368–372.

Keller, R., 2005. Cell migration during gastrulation. Current Opinion in Cell Biology. 17(5): 533–541.

Krueger, E. W., Orth, J. D., Cao, H., and McNiven, M. A., 2003. A dynamin-cortactin-Arp2/3 complex mediates actin reorganization in growth factor-stimulated cells. Mol Biol Cell 14(3): 1085–1096.

Kuo, J. C., 2013. Mechanotransduction at focal adhesions: Integrating cytoskeletal mechanics in migrating cells. Journal of Cellular and Molecular Medicine. 17(6): 704–712.

Larkins, C. E., Aviles, G. D. G., East, M. P., Kahn, R. A., and Caspary, T., 2011. Arl13b regulates ciliogenesis and the dynamic localization of Shh signaling proteins. Molecular Biology of the Cell 22(23): 4694–4703.

Le Clainche, C., and Carlier, M.-F., 2008. Regulation of actin assembly associated with protrusion and adhesion in cell migration. Physiological reviews 88(2): 489–513.

Letort, G., Ennomani, H., Gressin, L., Théry, M., and Blanchoin, L., 2015. Dynamic reorganization of the actin cytoskeleton. F1000Research 4(0): 1–11.

Li, 2013. Collective cell migration: Implications for wound healing and cancer invasion. Burns and Trauma 1(1): 21.

Linder, S., 2007. The matrix corroded: podosomes and invadopodia in extracellular matrix degradation. Trends in Cell Biology. 17(3): 107–117.

Liu, T., Ye, Y., Zhang, X., Zhu, A., Yang, Z., Fu, Y., Wei, C., Liu, Q., Zhao, C., and Wang, G., 2015. Downregulation of non-muscle myosinï¿½IIA expression inhibits migration and invasion of gastric cancer cells via the c-Jun N-terminal kinase signaling pathway. Molecular Medicine Reports 13(2): 1639–1644.

Locascio, A., and Nieto, M. A., 2001. Cell movements during vertebrate development: Integrated tissue behaviour versus individual cell migration. Current Opinion in Genetics and Development. 11(4): 464–469.

Luster, A. D., Alon, R., and von Andrian, U. H., 2005. Immune cell migration in inflammation: present and future therapeutic targets. Nature Immunology 6(12): 1182–1190.

Ma, X., and Adelstein, R. S., 2014. The role of vertebrate nonmuscle Myosin II in development and human disease. Bioarchitecture. 4(3): 88–102.

Mayor, R., and Etienne-Manneville, S., 2016. The front and rear of collective cell migration. Nature Reviews Molecular Cell Biology Nature Publishing Group 17(2): 97–109.

Mellström, K., Heldin, C. H., and Westermark, B., 1988. Induction of circular membrane ruffling on human fibroblasts by platelet-derived growth factor. Experimental Cell Research 177(2): 347–359.

Newell-Litwa, K. A., Horwitz, R., and Lamers, M. L., 2015. Non-muscle myosin II in disease: mechanisms and therapeutic opportunities. Disease Models & Mechanisms 8(12): 1495–1515.

Pasqualato, S., Renault, L., and Cherfils, J., 2002. Arf, Arl, Arp and Sar proteins: A family of GTP-binding proteins with a structural device for “front-back” communication. EMBO Reports 3(11): 1035–1041.

Petrie, R. J., Doyle, A. D., and Yamada, K. M., 2009. Random versus directionally persistent cell migration. Nature Reviews Molecular Cell Biology 10(8): 538–549.

Pollard, T. D., and Cooper, J. A., 2009. Actin, a Central Player in Cell Shape and Movement. Science 326(5957): 1208–1212.

Ponti, A., 2004. Two Distinct Actin Networks Drive the Protrusion of Migrating Cells. Science 305(5691): 1782–1786.

Porter, A. P., Papaioannou, A., and Malliri, A., 2016. Deregulation of Rho GTPases in cancer. Small GTPases 1248(May): 1–16.

Rayment, I., Holden, H. M., Whittaker, M., Yohn, C. B., Lorenz, M., Holmes, K. C., and Milligan, R. A., 1993a. Structure of the actin-myosin complex and its implications for muscle-contraction. Science 261(5117): 58.

Rayment, I., Rypniewski, W. R., Schmidt-Base, K., Smith, R., Tomchick, D. R., Benning, M. M., Winkelmann, D. A., Wesenberg, G., and Holden, H. M., 1993b. Three-dimensional structure of myosin subfragment-1: a molecular motor. Science (New York, N.Y.) 261(5117): 50–58.

Sandquist, J. C., and Means, A. R., 2008. The C-terminal tail region of nonmuscle myosin II directs isoform-specific distribution in migrating cells. Molecular biology of the cell 19(12): 5156–5167.

Sandquist, J. C., Swenson, K. I., DeMali, K. A., Burridge, K., and Means, A. R., 2006. Rho kinase differentially regulates phosphorylation of nonmuscle myosin II isoforms A and B during cell rounding and migration. Journal of Biological Chemistry 281(47): 35873–35883.

Schmidt, A., and Hall, A., 2002. Guanine nucleotide exchange factors for Rho GTPases: turning on the switch. Genes & development 16(13): 1587–1609.

Scholey, J. M., Taylor, K. A., and Kendrick-Jones, J., 1980. Regulation of non-muscle myosin assembly by calmodulin-dependent light chain kinase. Nature. 287(5779): 233–235.

Schroeder, A., Heller, D. A., Winslow, M. M., Dahlman, J. E., Pratt, G. W., Langer, R., Jacks, T., and Anderson, D. G., 2011. Treating metastatic cancer with nanotechnology. Nature Reviews Cancer 12(1): 39–50.

Seixas, E., Barros, M., Seabra, M. C., and Barral, D. C., 2013. Rab and Arf proteins in genetic diseases. Traffic. 14(8): 871–885.

Sero, J. E., Thodeti, C. K., Mammoto, A., Bakal, C., Thomas, S., and Ingber, D. E., 2011. Paxillin mediates sensing of physical cues and regulates directional cell motility by controlling lamellipodia positioning. PLoS ONE 6(12):.

Shao, J., Xu, L., Chen, L., Lu, Q., Xie, X., Shi, W., Xiong, H., Shi, C., Huang, X., Mei, J., Rao, H., Lu, H., Lu, N., and Luo, S., 2017. Arl13b Promotes Gastric Tumorigenesis by Regulating Smo Trafficking and Activation of the Hedgehog Signaling Pathway. Cancer Research 77(15): 4000–4013.

Simanshu, D. K., Nissley, D. V., and McCormick, F., 2017. RAS Proteins and Their Regulators in Human Disease. Cell. 170(1): 17–33.

Small, J. V., Stradal, T., Vignal, E., and Rottner, K., 2002. The lamellipodium: Where motility begins. Trends in Cell Biology. 12(3): 112–120.

Somlyo, A. P. A. V. P., and Somlyo, A. P. A. V. P., 2003. Ca2+ sensitivity of smooth muscle and nonmuscle myosin II: modulated by G proteins, kinases, and myosin phosphatase. Physiol Rev 83(4): 1325–1358.

Soule, H. D., Maloney, T. M., Wolman, S. R., Peterson, W. D., Brenz, R., McGrath, C. M., Russo, J., Pauley, R. J., Jones, R. F., and Brooks, S. C., 1990. Isolation and characterization of a spontaneously immortalized human breast epithelial cell line, MCF-10. Cancer Research 50(18): 6075–6086.

Soule, H. D., Vazquez, J., Long, A., Albert, S., and Brennan, M., 1973. A human cell line from a pleural effusion derived from a breast carcinoma. Journal of the National Cancer Institute 51(5): 1409–1416.

Thomas, S., Cantagrel, V., Mariani, L., Serre, V., Lee, J.-E., Elkhartoufi, N., de Lonlay, P., Desguerre, I., Munnich, A., Boddaert, N., Lyonnet, S., Vekemans, M., Lisgo, S. N., Caspary, T., Gleeson, J., and Attié-Bitach, T., 2015. Identification of a novel ARL13B variant in a Joubert syndrome-affected patient with retinal impairment and obesity. European journal of human genetics : EJHG 23(5): 621–627.

Tojkander, S., Gateva, G., and Lappalainen, P., 2012. Actin stress fibers--assembly, dynamics and biological roles. Journal of cell science 125(Pt 8): 1855–1864.

Umemoto, S., Bengur, A. R., and Sellers, J. R., 1989. Effect of multiple phosphorylations of smooth muscle and cytoplasmic myosins on movement in an in vitro motility assay. Journal of Biological Chemistry 264(3): 1431–1436.

Vicente-Manzanares, M., and Horwitz, A. R., 2010. Myosin light chain mono- and di-phosphorylation differentially regulate adhesion and polarity in migrating cells. Biochemical and Biophysical Research Communications 402(3): 537–542.

Vicente-Manzanares, M., Ma, X., Adelstein, R. S., and Horwitz, a. R., 2009. Non-muscle myosin II takes centre stage in cell adhesion and migration. Nature Reviews Molecular Cell Biology 10(11): 778–790.

Vicente-Manzanares, M., Zareno, J., Whitmore, L., Choi, C. K., and Horwitz, A. F., 2007. Regulation of protrusion, adhesion dynamics, and polarity by myosins IIA and IIB in migrating cells. Journal of Cell Biology 176(5): 573–580.

Wang, W., Goswami, S., Sahai, E., Wyckoff, J. B., Segall, J. E., and Condeelis, J. S., 2005. Tumor cells caught in the act of invading: Their strategy for enhanced cell motility. Trends in Cell Biology. 15(3): 138–145.

Winkelmann, D. A., Almeda, S., Vibert, P., and Cohen, C., 1984. A new myosin fragment: visualization of the regulatory domain. Nature 307(5953): 758–760.

Wolfenson, H., Lavelin, I., and Geiger, B., 2013. Dynamic Regulation of the Structure and Functions of Integrin Adhesions. Developmental Cell. 24(5): 447–458.

Yamaguchi, H., and Condeelis, J., 2007. Regulation of the actin cytoskeleton in cancer cell migration and invasion. Biochimica et Biophysica Acta - Molecular Cell Research. 1773(5): 642–652.

Supplementary information

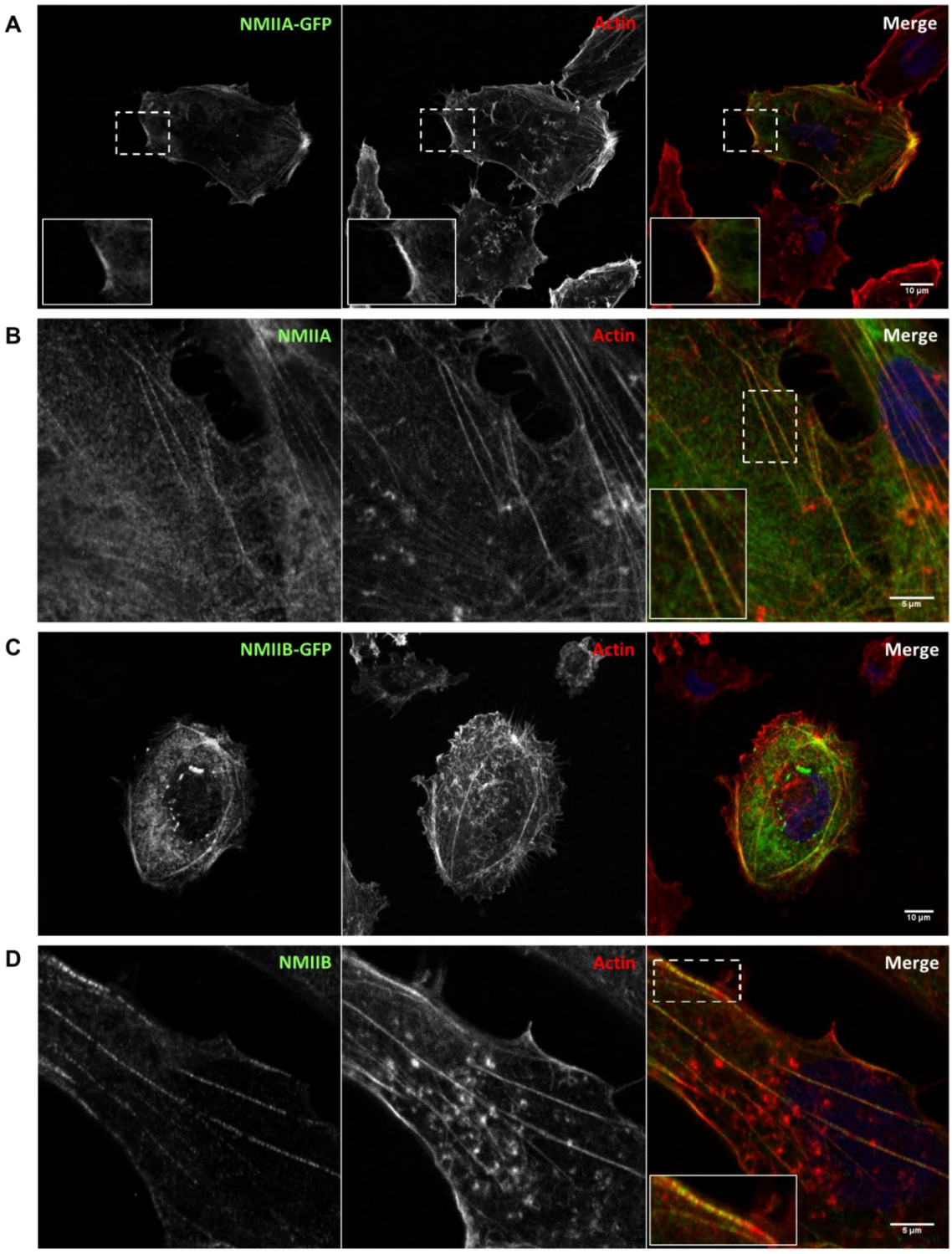

Figure S1 – NMIIA and NMIIB co-localize with actin in MDA-MB-231 cells. MDA-MB-231 cells overexpressing NMIIA-GFP or NMIIB-GFP were fixed and stained with Alexa-Fluor-568-conjugated phalloidin. (A and B) NMIIA co-localizes with actin structures. (C and D) NMIIB co-localizes with actin structures. A periodic pattern of alternating actin and NMIIA (B) or NMIIB (D) can be seen in the cells' stress fibers. Enlarged views of the indicated sections are shown in the insets. All images correspond to representative Z stacks obtained by confocal microscopy. Scale bars: (A and C) 10 µm; (B and D) 5 µm.

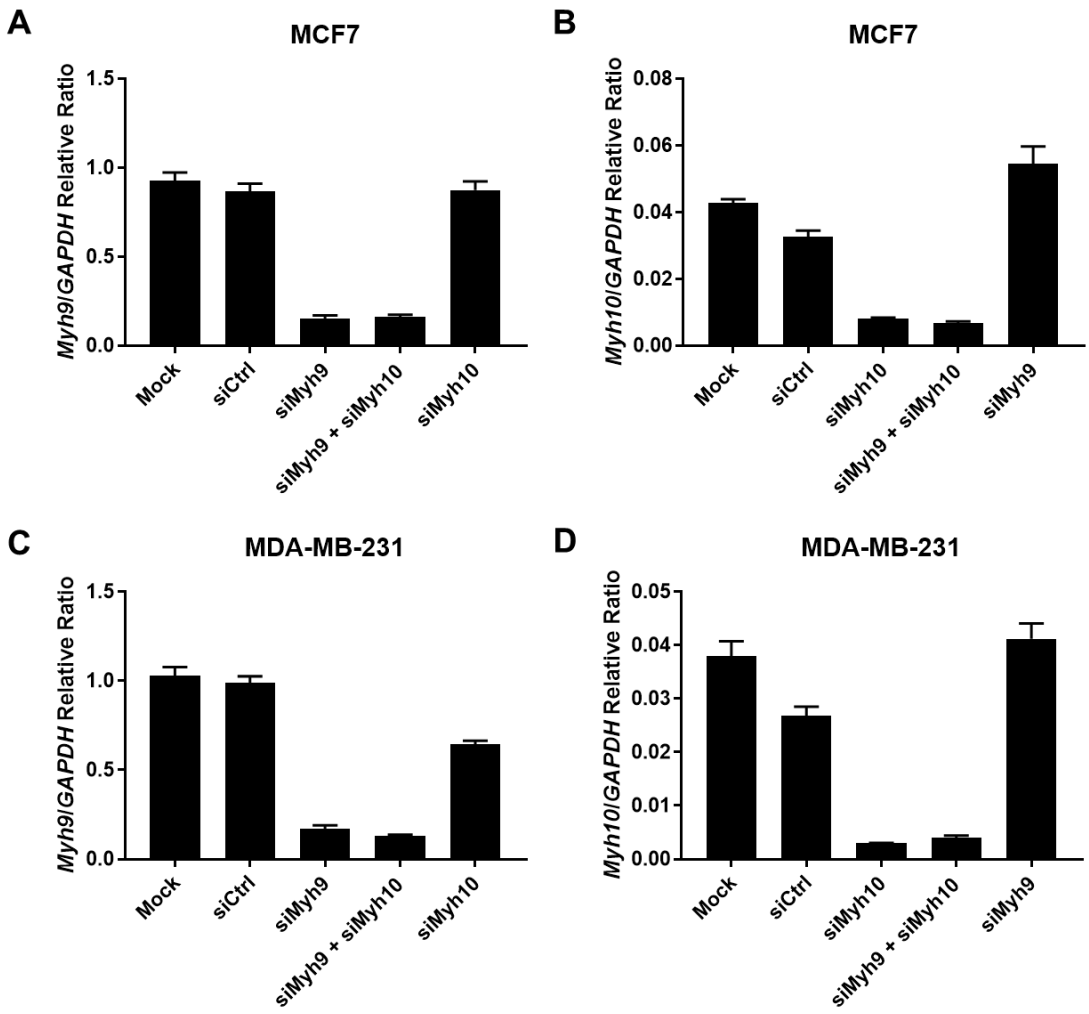

Figure S2 – Quantification of NMIIA and/or NMIIB mRNA levels by RT-qPCR. MCF7 or MDA-MB-231 cells silenced for NMIIA and/or NMIIB were collected at the end of the wound healing assays (approximately 72 hours post-transfection). Silencing of NMIIA **(A and C)** or NMIIB **(B and D)** by siRNA on MCF7 **(A and B)** and MDA-MB-231 **(C and D)** cells was confirmed by analysis of mRNA levels through RT-qPCR. The expression of each gene (*MYH9* and *MYH10*, respectively) was normalized to the expression of *GAPDH*, a housekeeping gene. Results represent the relative ratios between expression of *MYH9* or *MYH10* and *GAPDH* and are represented as mean ± standard deviation of three replicates.

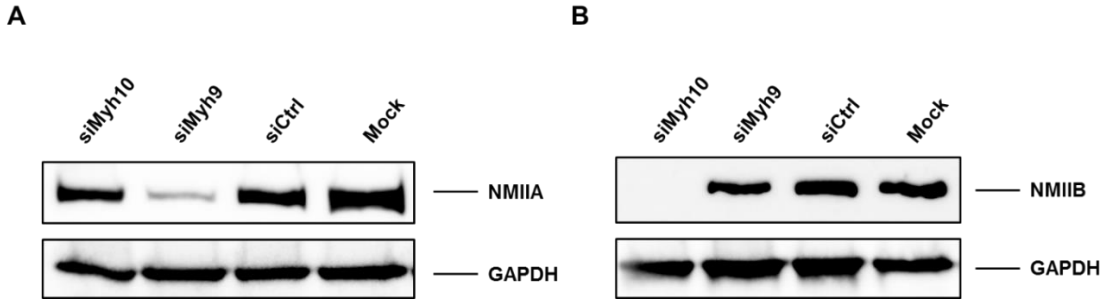

Figure S3 – Quantification of NMIIA and/or NMIIB protein levels by Western Blot. MDA-MB-231 cells silenced for NMIIA and/or NMIIB were collected after the wound healing assays (approximately 72 hours post-transfection). Silencing of NMIIA **(A)** or NMIIB **(B)** was confirmed by Western Blot. Protein extracts were obtained using a lysis buffer containing 0,1% IGEPAL and 40 µg of total cell extract were run on 8% SDS-PAGE. The membranes were incubated with anti-NMIIA (A) or anti-NMIIB (B) and anti-GAPDH (loading control) antibodies, before incubation with the respective secondary antibodies.